

PL-TR-93-2078

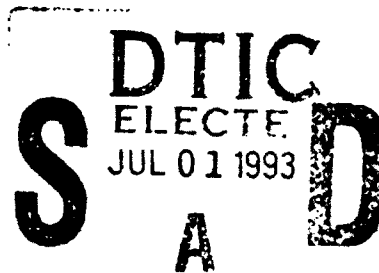
AD-A266 405



**Full Waveform Inversion for Structure and Source
Parameters Using Regional Data Recorded in
Eastern Kazakhstan**

Danny J. Harvey

University of Colorado
Department of Physics
JSPC/TAGG
Campus Box 583
Boulder, CO 80309-0583



1 April 1993

Final Report

1 September 1990 - 1 September 1992

Approved for public release; distribution unlimited

93-14995



PHILLIPS LABORATORY
Directorate of Geophysics
AIR FORCE MATERIEL COMMAND
HANSCOM AIR FORCE BASE, MA 01731-3010

93 6 30 061

The views and conclusions contained in this document are those of the authors and should not be interpreted as representing the official policies, either expressed or implied, of the Air Force or the U.S. Government.

This technical report has been reviewed and is approved for publication.



JAMES F. LEWKOWICZ
Contract Manager
Solid Earth Geophysics Branch
Earth Sciences Division



JAMES F. LEWKOWICZ
Branch Chief
Solid Earth Geophysics Branch
Earth Sciences Division



DONALD H. ECKHARDT, Director
Earth Sciences Division

This document has been reviewed by the ESD Public Affairs Office (PA) and is releasable to the National Technical Information Service (NTIS).

Qualified requestors may obtain additional copies from the Defense Technical Information Center. All others should apply to the National Technical Information Service.

If your address has changed, or if you wish to be removed from the mailing list, or if the addressee is no longer employed by your organization, please notify PL/TSI, Hanscom AFB MA 01731-3010. This will assist us in maintaining a current mailing list.

Do not return copies of this report unless contractual obligations or notices on a specific document requires that it be returned.

REPORT DOCUMENTATION PAGE

Form Approved
OMB No 0704-0188

Public reporting burden for this collection of information is estimated to average 1 hour per response, including the time for reviewing instructions, searching existing data sources, gathering and maintaining the data needed, and completing and reviewing the collection of information. Send comments regarding this burden estimate or any other aspect of this collection of information, including suggestions for reducing this burden, to Washington Headquarters Services, Directorate for Information Operations and Reports, 1215 Jefferson Davis Highway, Suite 1204, Arlington, VA 22202-4302, and to the Office of Management and Budget, Paperwork Reduction Project (0704-0188), Washington, DC 20503.

1. AGENCY USE ONLY (Leave blank)		2. REPORT DATE 1 April 1993	3. REPORT TYPE AND DATES COVERED Final Report 1 Sept 1990 - 1 Sept 1992
4. TITLE AND SUBTITLE Full Waveform Inversion for Structure and Source Parameters Using Regional Data Recorded in Eastern Kazakhstan			5. FUNDING NUMBERS F19628-90-K-0050 PE62101F PR 7600 TA09 WV BH
6. AUTHOR(S) Danny J. Harvey			8. PERFORMING ORGANIZATION REPORT NUMBER
7. PERFORMING ORGANIZATION NAME(S) AND ADDRESS(ES) The University of Colorado Department of Physics JSPG/TAGG Boulder, CO 80309-0583			10. SPONSORING MONITORING AGENCY REPORT NUMBER PL-TR-93-2078
9. SPONSORING/MONITORING AGENCY NAME(S) AND ADDRESS(ES) Phillips Laboratory 29 Randolph Road Hanscom AFB, MA 01731-3010 Contract Manager: James Lewkowicz/GPEH			11. SUPPLEMENTARY NOTES
12a. DISTRIBUTION/AVAILABILITY STATEMENT approved for public release; distribution unlimited			12b. DISTRIBUTION CODE
13. ABSTRACT (Maximum 200 words) We have completed a study which was aimed at obtaining fundamental understanding of regional wave propagation by attempting to match synthetic seismograms with real data. The first part of this study involved the identification and analysis of a set of local and regional seismic events recorded near the former Soviet test site at Semipalatinsk. We then applied full waveform inversion in the 0.5 to 1 Hertz frequency band to selected events to extract source and structure parameters. We found that for certain source-receiver paths we could do an excellent job of matching complete seismograms on radial and vertical components up to a frequency of one Hertz including P, S and Rg phases using shallow explosion sources. For other source-receiver paths the fits were not so good using shallow explosion sources, however we obtained good fits on all three components by assuming a 5 km deep earthquake source. These results indicate that waveform inversion can be used to discriminate small shallow explosions from small relatively shallow earthquakes and that structural effects can be accurately modeled in this region up to a frequency of 1 Hertz.			
14. SUBJECT TERMS Regional Events Source Discrimination Waveform Inversion Waveform Modeling			15. NUMBER OF PAGES 54
			16. PRICE CODE
17. SECURITY CLASSIFICATION OF REPORT UNCLASSIFIED	18. SECURITY CLASSIFICATION OF THIS PAGE UNCLASSIFIED	19. SECURITY CLASSIFICATION OF ABSTRACT UNCLASSIFIED	20. LIMITATION OF ABSTRACT SAR

Table of Contents

1.	INTRODUCTION	1
2.	DATA AND OBSERVATIONS	2
	2.1 Event Determination	3
	2.2 Data Characterization	3
	2.3 Data Analysis	17
3.	INVERSION PROCESS	24
	3.1 Rg Dispersion Inversion	24
	3.2 Full Waveform Inversion	25
4.	INVERSION RESULTS AND APPLICATION TO OTHER EVENTS	30
5.	CONCLUSIONS	39
6.	CONTRIBUTING RESEARCHERS	41
7.	RELATED CONTRACTS AND PUBLICATIONS	41
8.	REFERENCES	41

DTIC QUARTERLY COLLECTION 5

Accession For	
NTIS	GRAND
DTIC	TAB
Unannounced	□
Justification	□
By	
Distribution/	
Availability Codes	
Dist	Avail. and/or Special
A-1	

Full Waveform Inversion for Structure and Source Parameters Using Regional Data Recorded in Eastern Kazakhstan

by

Danny J. Harvey

1. Introduction

The technical problems associated with monitoring clandestine nuclear testing in the context of the new world order have caused a significant redirection of research efforts in seismology. The old scenario, involving underground tests by a handful of nuclear powers in predominantly a few well known test sites, was handled with a monitoring strategy that consisted primarily of empirical calibration, which worked reasonably well given the nature of the testing. In the context of nuclear non-proliferation, however, we have discovered that there are many gaps in our fundamental understanding of seismic wave propagation at high frequencies in the types of complex geologic settings that will be encountered. We will not be able to depend upon large databases of prior direct experience to confidently detect and discriminate a first test from an emerging nuclear power.

We have completed a study which was aimed at obtaining fundamental understanding of regional wave propagation by attempting to match synthetic seismograms with real data. In the process we have learned much about the behavior of P, S, Lg and Rg and how they relate to earth structure, source characteristics and source-receiver geometry. In this report we will document a two phase study in which we identified and analyzed a set of local and regional seismic events recorded near the former Soviet test site at Semipalatinsk. We then applied full waveform inversion to selected events to extract source and structure parameters. We found that for certain

source-receiver paths we could do a very good job of matching complete seismograms on radial and vertical components up to a frequency of one Hertz including P, S and Rg phases using shallow explosion sources. For other source-receiver paths the fits were not so good using shallow explosion sources, however we obtained good fits on all three components by assuming a 5 km deep earthquake source. These results indicate that waveform inversion can be used to discriminate small shallow explosions from small relatively shallow earthquakes.

2. Data and Observations

We used seismic data recorded as part of the NRDC program conducted during 1987. The NRDC network was operated by the University of California, San Diego and consisted of three stations that surrounded the Shagan River and Degelen Mountain areas of the Eastern Kazakhstan Soviet test site. Although there were three stations in the NRDC network, throughout most of the year only one or two stations were operational and the most consistent station was KKL (Karkaralinsk). All of the results in this study are based upon data collected at KKL. We used as our data source the NRDC Information Product which was compiled by IRIS' Joint Seismic Program Center and distributed through the IRIS Data Management Center.

The instrumentation at KKL consisted of surface 1 Hz 3-component seismometers and a borehole 0.2 Hz 3-component seismometer all recording at two different gain levels (on 16-bit digitizers) and at 250 sps. The site was on granitic bedrock and generally exhibited low noise characteristics. All of the results presented in this study are based upon the borehole instruments that were at a depth of 100 m.

The region around KKL is an active mining area with many shallow explosions and generally exhibits low natural seismicity. Most seismicity in the area is of the "induced" type and is associated with the large nuclear explosions at the former Soviet test site.

2.1 Event Determination

A total of 69 events were used in this study. These events were determined by scanning through one year's worth of data recorded at KKL looking for any events that had clearly identifiable P and S arrivals and whose S-P times were consistent with distances of less than 500 km. Measured S-P times were used to determine the distance of the event based upon the travel times used by Thurber¹. Event epicenters were determined by using the S-P distances along with back azimuth estimates that were obtained from polarization analysis. All events were assumed, initially, to be shallow mining blasts. A map of the 69 events used in this study is shown in Figure 1.

Although the epicenters determined from a single station location are subject to some scepticism, we think that they are fairly good as indicated by the clustering that would be characteristic of mining operations especially to the west, south and southwest. As we will show, these directions also correspond to the source-receiver paths for which we can fit the data. The locations to the north however are not particularly clustered, even though we know that this is an active mining region. This direction also represents source-receiver paths for which we have difficulty fitting synthetic seismograms to the data.

2.2 Data Characterization

Figure 2 shows the unfiltered KKL vertical components for all events sorted by azimuth and distance. All of the times are relative to the first P arrival time. The labels on the left of each trace give the distance and back azimuth in degrees to each event which can be used to identify the events in Figure 1. Probably the most interesting characteristic of the data that can be seen from this figure is the great variability in the excitation of Rg. If one looks carefully at the data it appears that events to the south

¹ Thurber, C., Given, H., Berger, J., Regional seismic event location with a sparse network: application to Eastern Kazakhstan, USSR, *J. Geophys. Res.* **94**, 17767-17780, 1989.

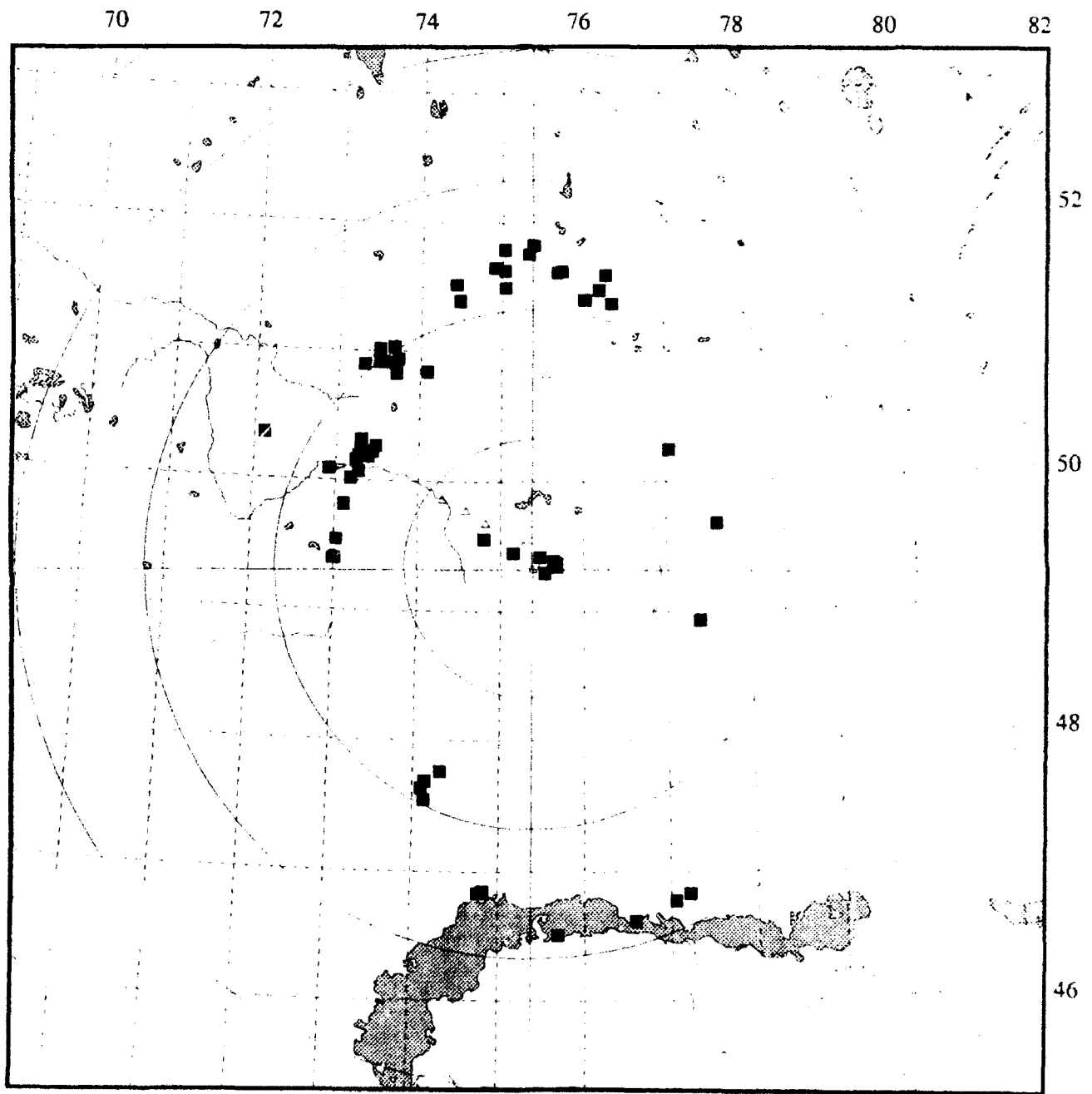


Figure 1. Event map centered at station KKL. Squares are events and triangles are stations. Circles are at one degrees distances from KKL.

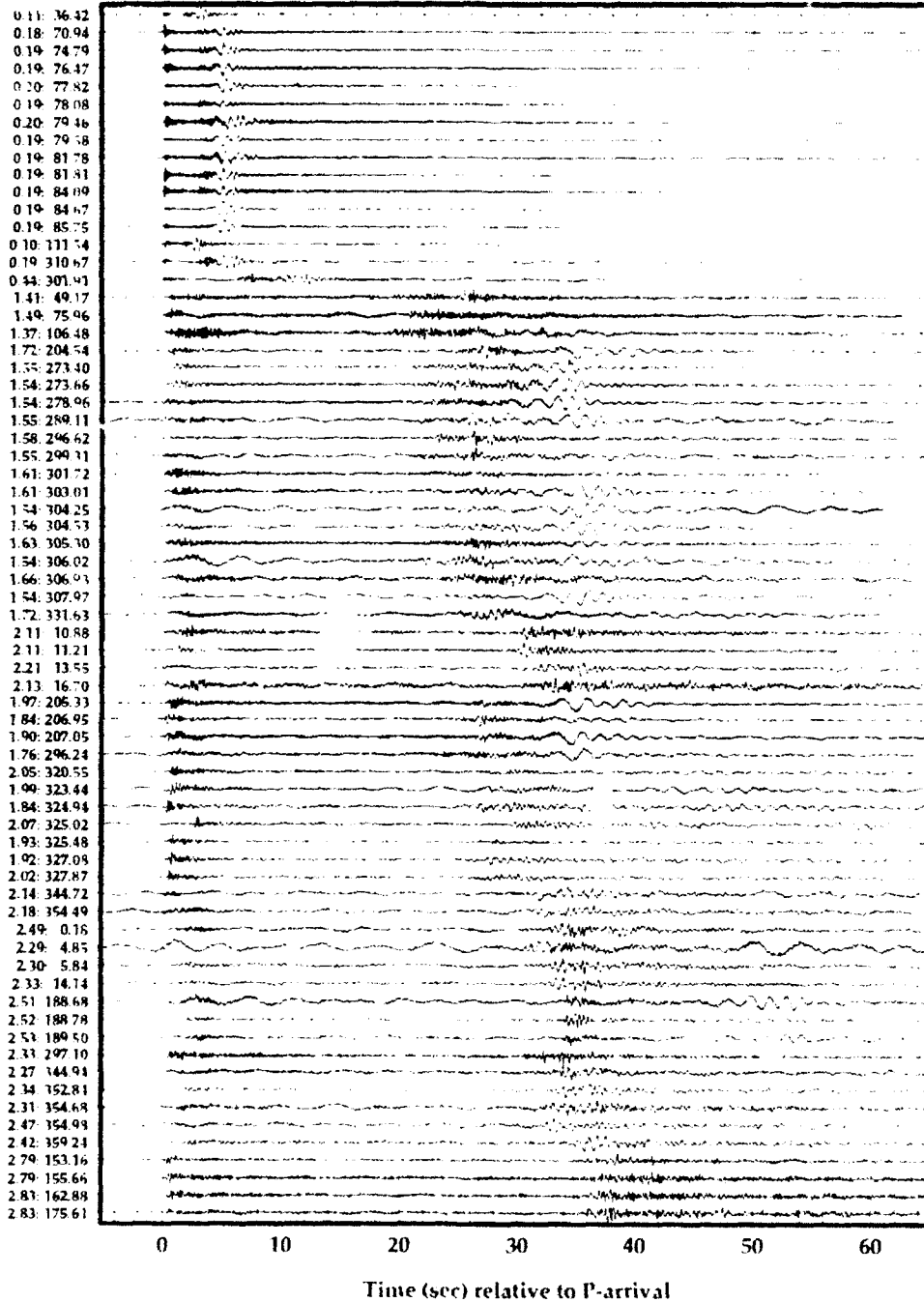


Figure 2. Unfiltered vertical component seismograms recorded by the borehole instrument at station KKL for the 69 events used in this study. Distance and back azimuth in degrees are given for each trace.

and west systematically show larger Rg amplitudes than events to the north or east (with the exception of the very local events).

In order to more clearly show the data we have split up Figure 2 into events coming from the same general regions which are shown in Figures 3 through 7. Each of these figures are split into unfiltered and filtered versions. The filtered versions were all filtered with a 6th order 0.5 to 1.0 Hz minimum phase Butterworth bandpass filter.

The local events (from about 10 to 50 km) are shown in Figures 3a and 3b. These all show high signal to noise with strong Rg excitation. Although not plotted here, the transverse components tend to show strong Love wave excitation as well. These data show that the near receiver environment is conducive to efficient Rg propagation and that the SH energy that we typically observe in explosion seismograms can be generated in large part at or near the source.

Events to the east and north are shown in Figures 4a and 4b. The signal to noise ratio is considerably lower than for the local events and there are no apparent Rg phases in the unfiltered data. After filtering, Rg phases appear on two of the easterly events, however it would be difficult to pick Rg on any of the other events.

Events to the northwest are shown in Figures 5a and 5b. These events seem to be generally more energetic than those to the north and east even though they are in the same general distance range. Another difference is that the Rg phases can be seen in more of the unfiltered traces and can be clearly seen in all of the filtered traces where they are consistently larger than either the P or S arrivals.

Events to the west are shown in Figures 6a and 6b. These are also relatively energetic events and the Rg phases generally can be clearly seen in the unfiltered data. The filtered traces, for the most part, show very strong Rg excitation that is usually much larger than either the P or S arrivals. The major exception to this is the most distant event which corresponds to one of the large chemical explosions (10 ton) that was detonated as part of the NRDC program.

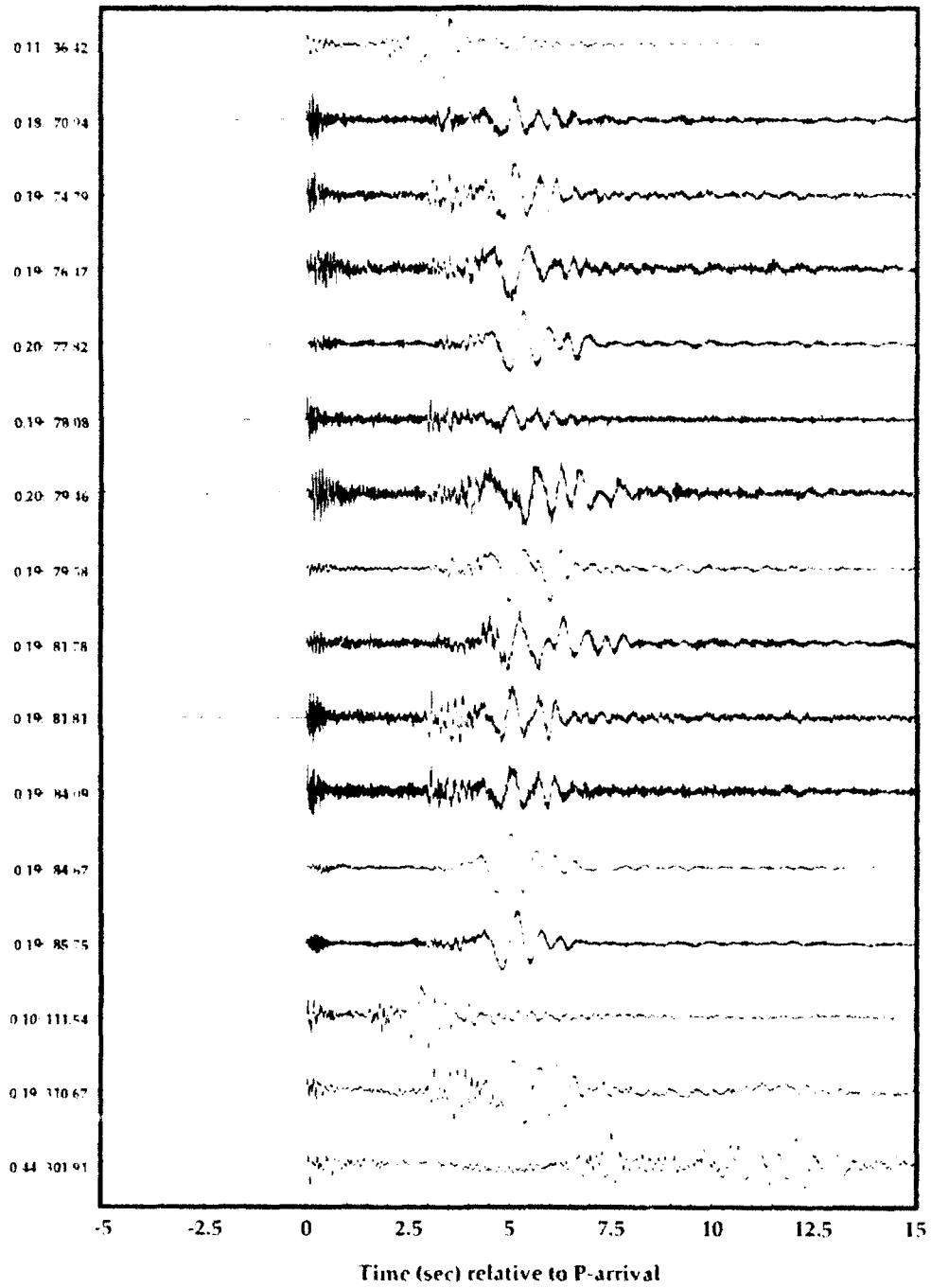


Figure 3a. Unfiltered vertical component seismograms recorded by the borehole instrument at station KKL for the local events used in this study. Distance and back azimuth in degrees are given for each trace.

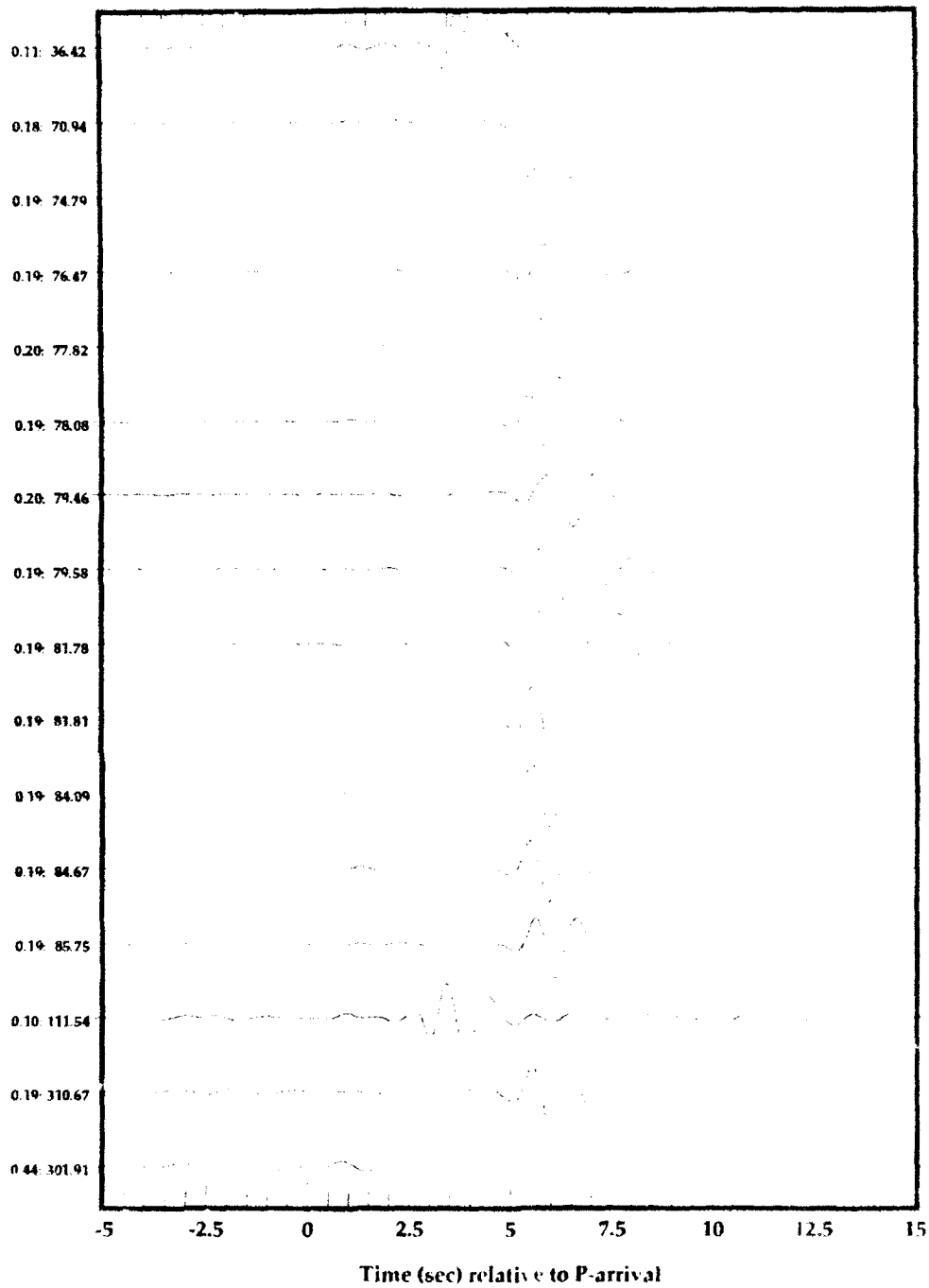


Figure 3b. 0.5 to 1.0 Hz bandpass filtered vertical component seismograms recorded by the borehole instrument at station KKL for the local events used in this study. Distance and back azimuth in degrees are given for each trace.

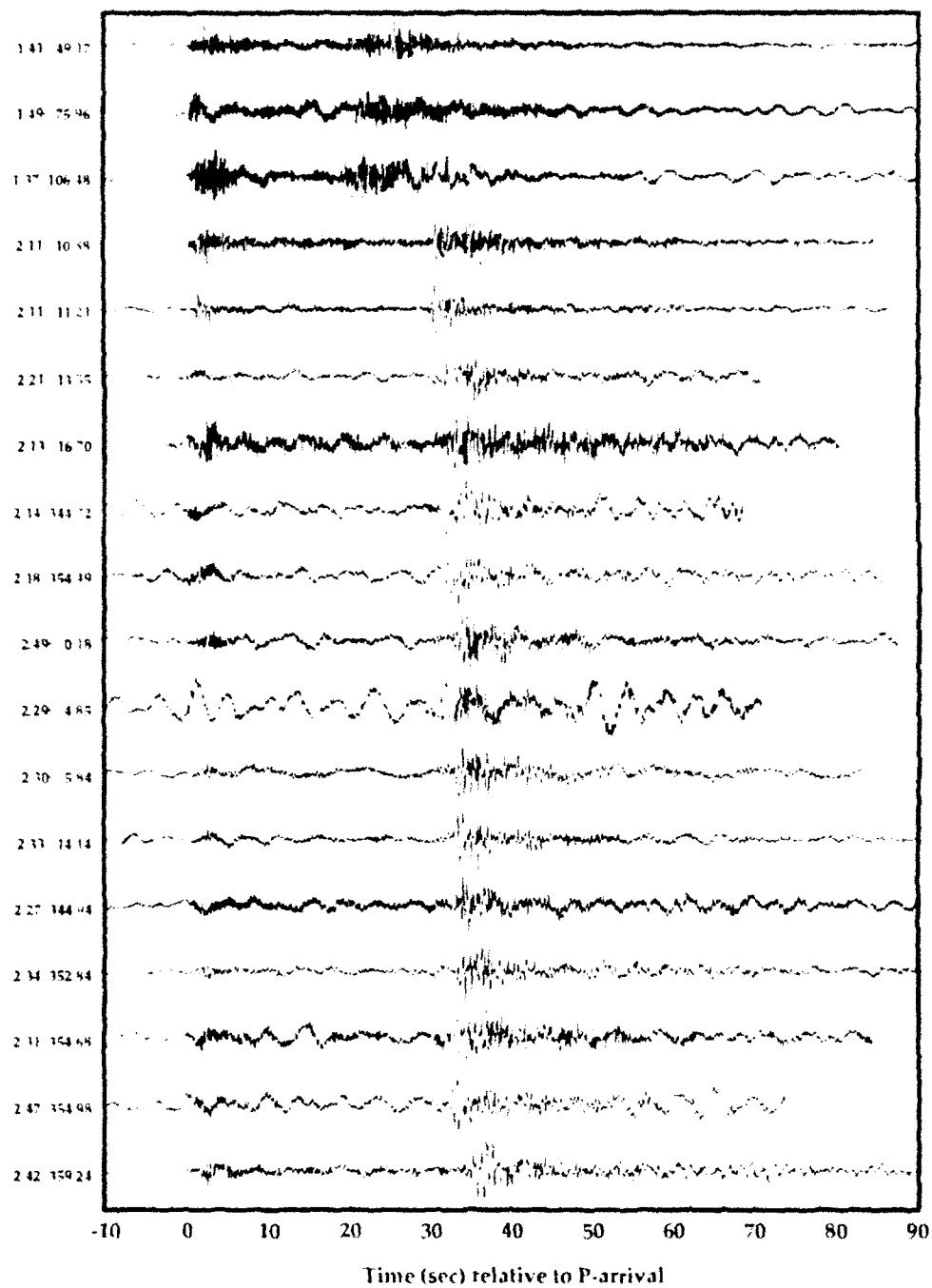


Figure 4a. Unfiltered vertical component seismograms recorded by the borehole instrument at station KKL for events to the east and north. Distance and back azimuth in degrees are given for each trace.

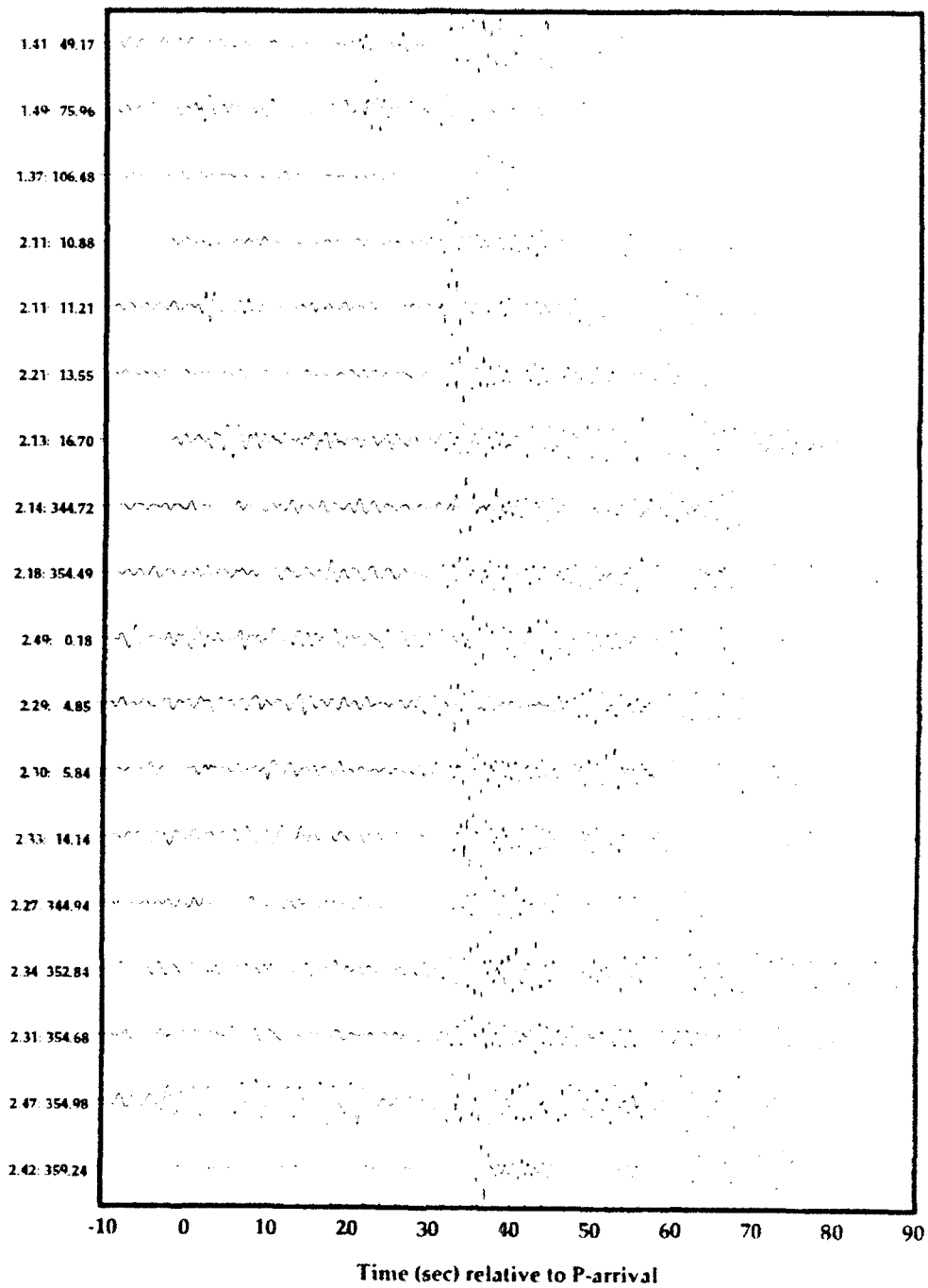


Figure 4b. 0.5 to 1.0 Hz bandpass filtered vertical component seismograms recorded by the borehole instrument at station KKL for events to the east and north. Distance and back azimuth in degrees are given for each trace.

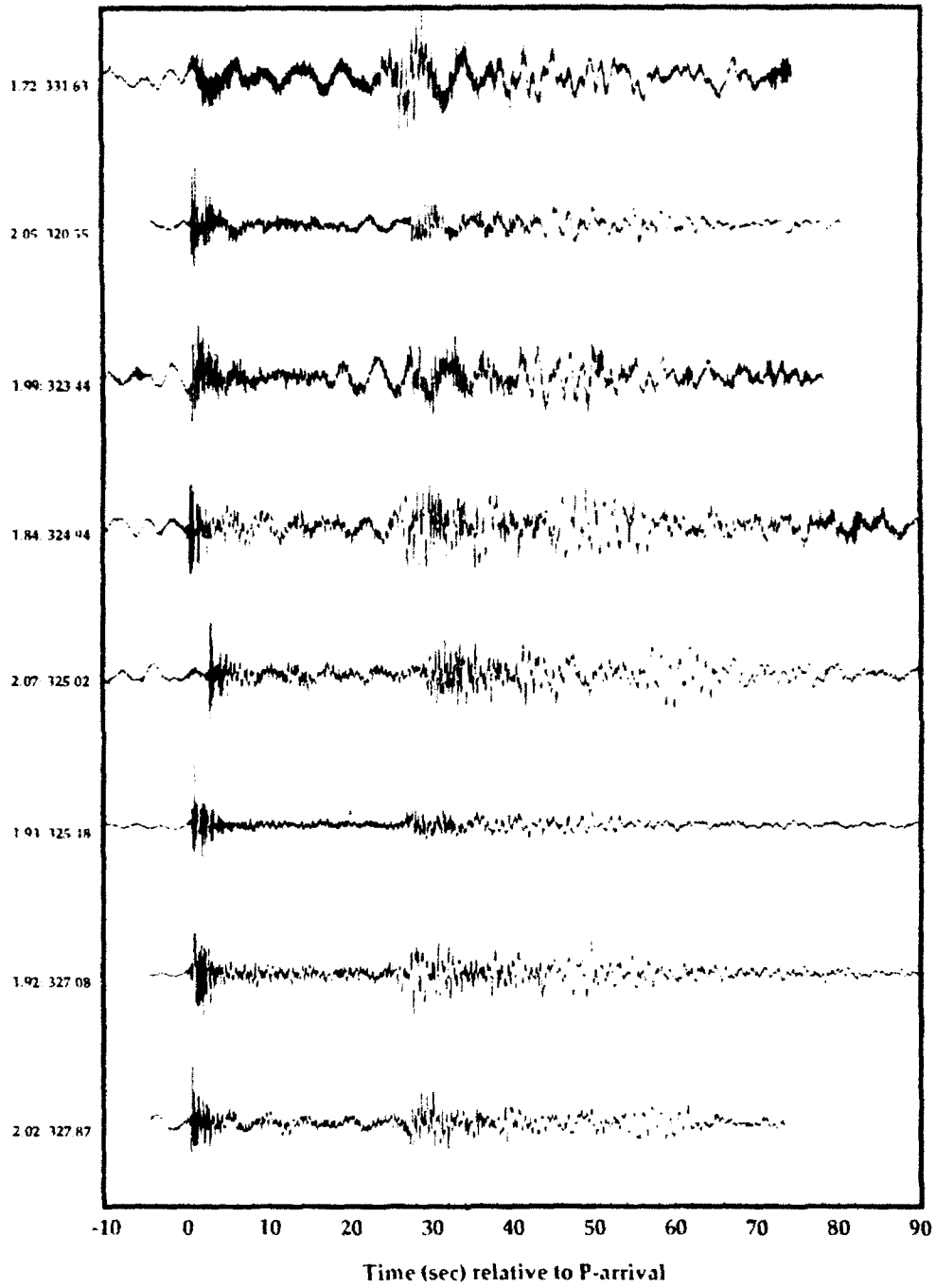


Figure 5a. Unfiltered vertical component seismograms recorded by the borehole instrument at station KKL for events to the northwest. Distance and back azimuth in degrees are given for each trace.

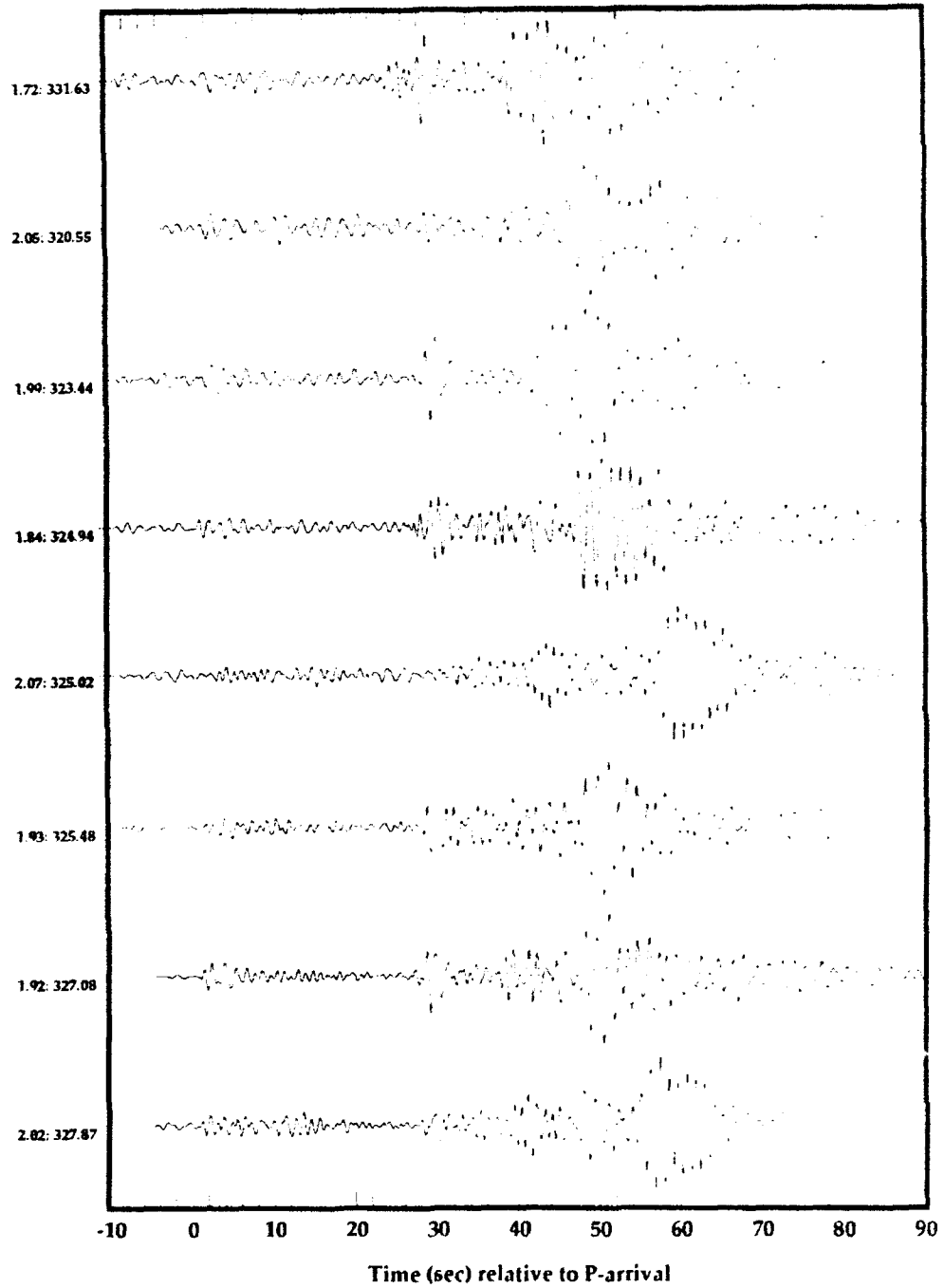


Figure 5b. 0.5 to 1.0 Hz bandpass filtered vertical component seismograms recorded by the borehole instrument at station KKL for events to the northwest. Distance and back azimuth in degrees are given for each trace.

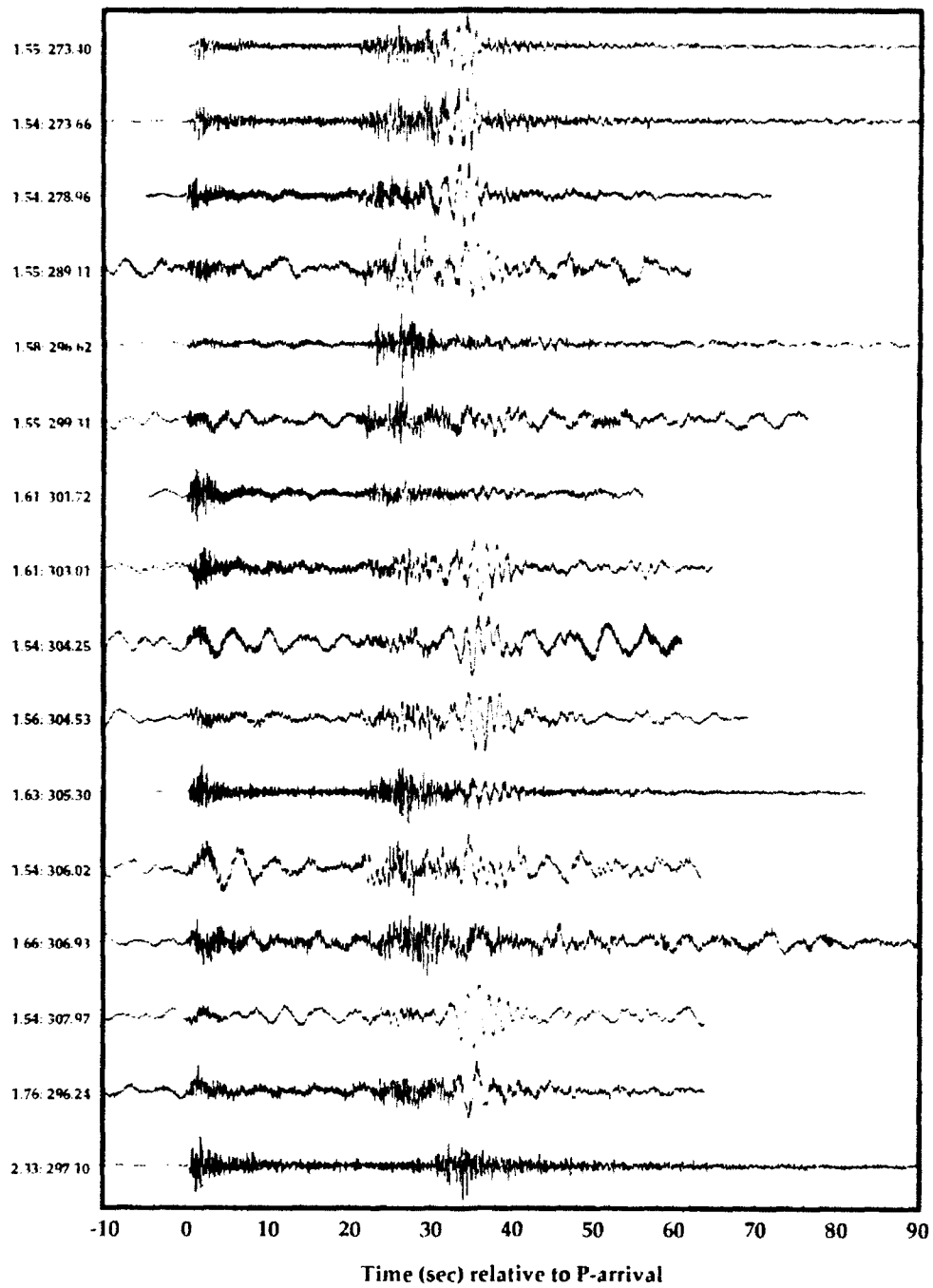


Figure 6a. Unfiltered vertical component seismograms recorded by the borehole instrument at station KKL for events to the west. Distance and back azimuth in degrees are given for each trace.

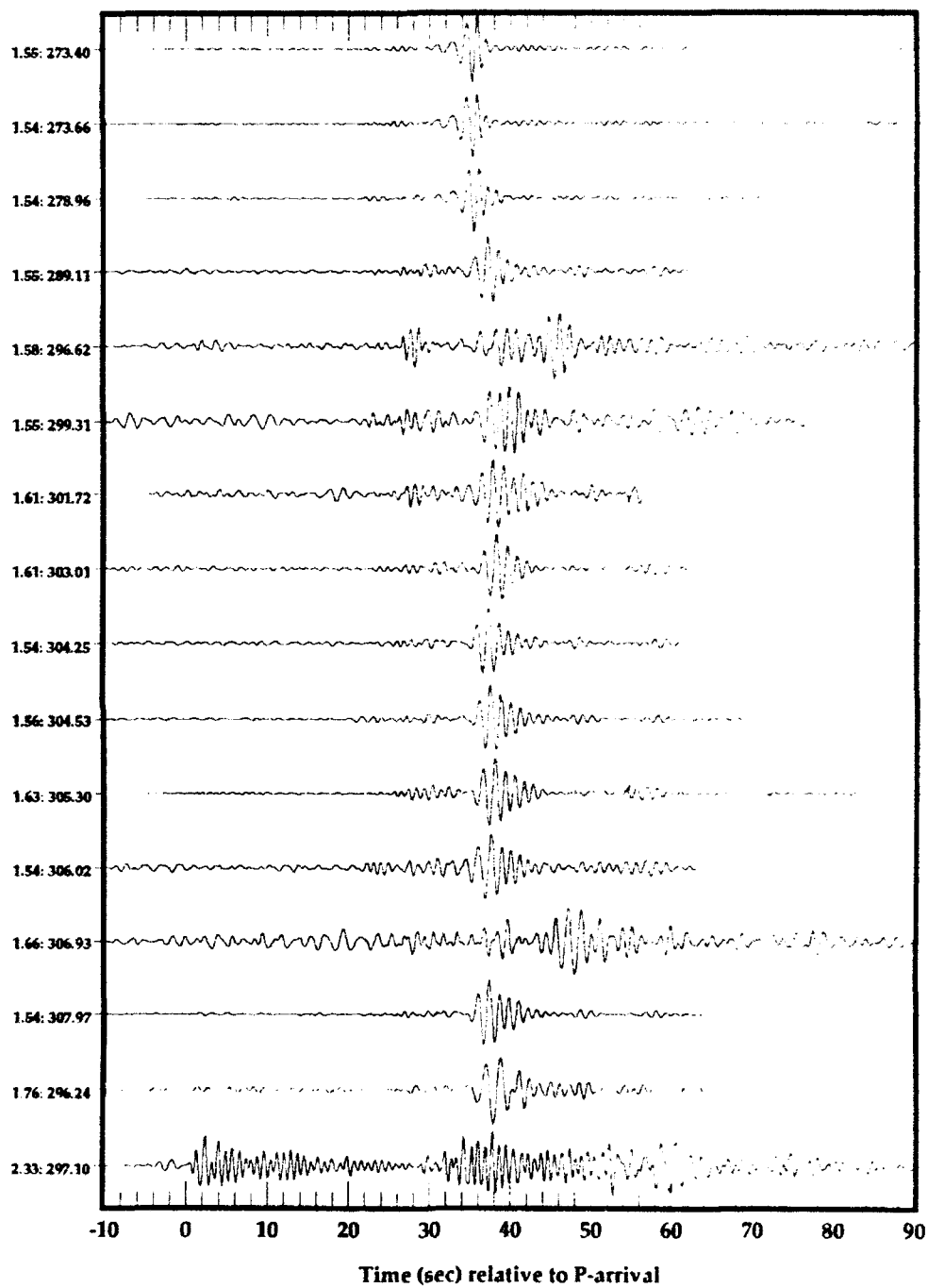


Figure 6b. 0.5 to 1.0 Hz bandpass filtered vertical component seismograms recorded by the borehole instrument at station KKL for events to the west. Distance and back azimuth in degrees are given for each trace.

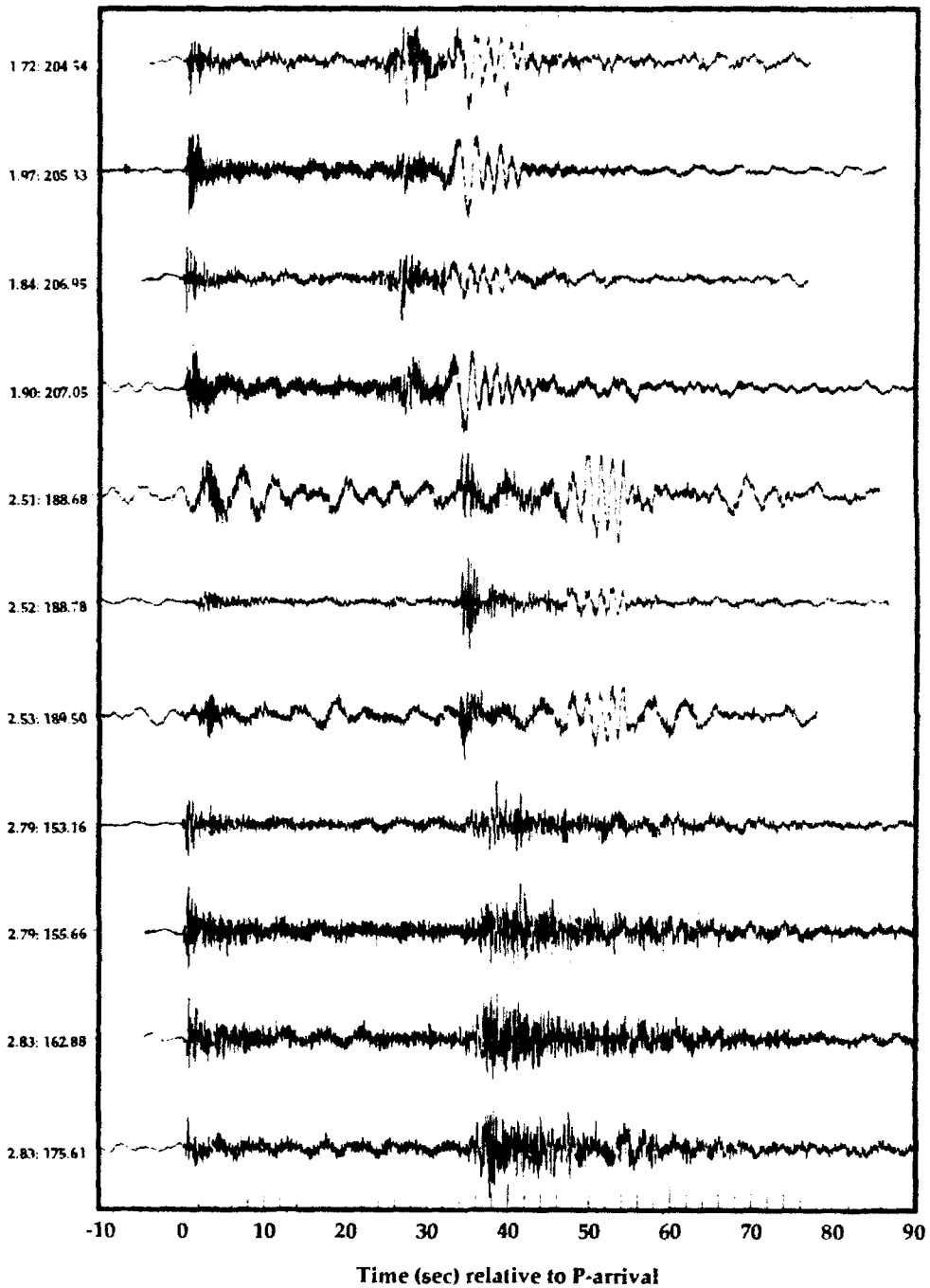


Figure 7a. Unfiltered vertical component seismograms recorded by the borehole instrument at station KKL for events to the south. Distance and back azimuth in degrees are given for each trace.

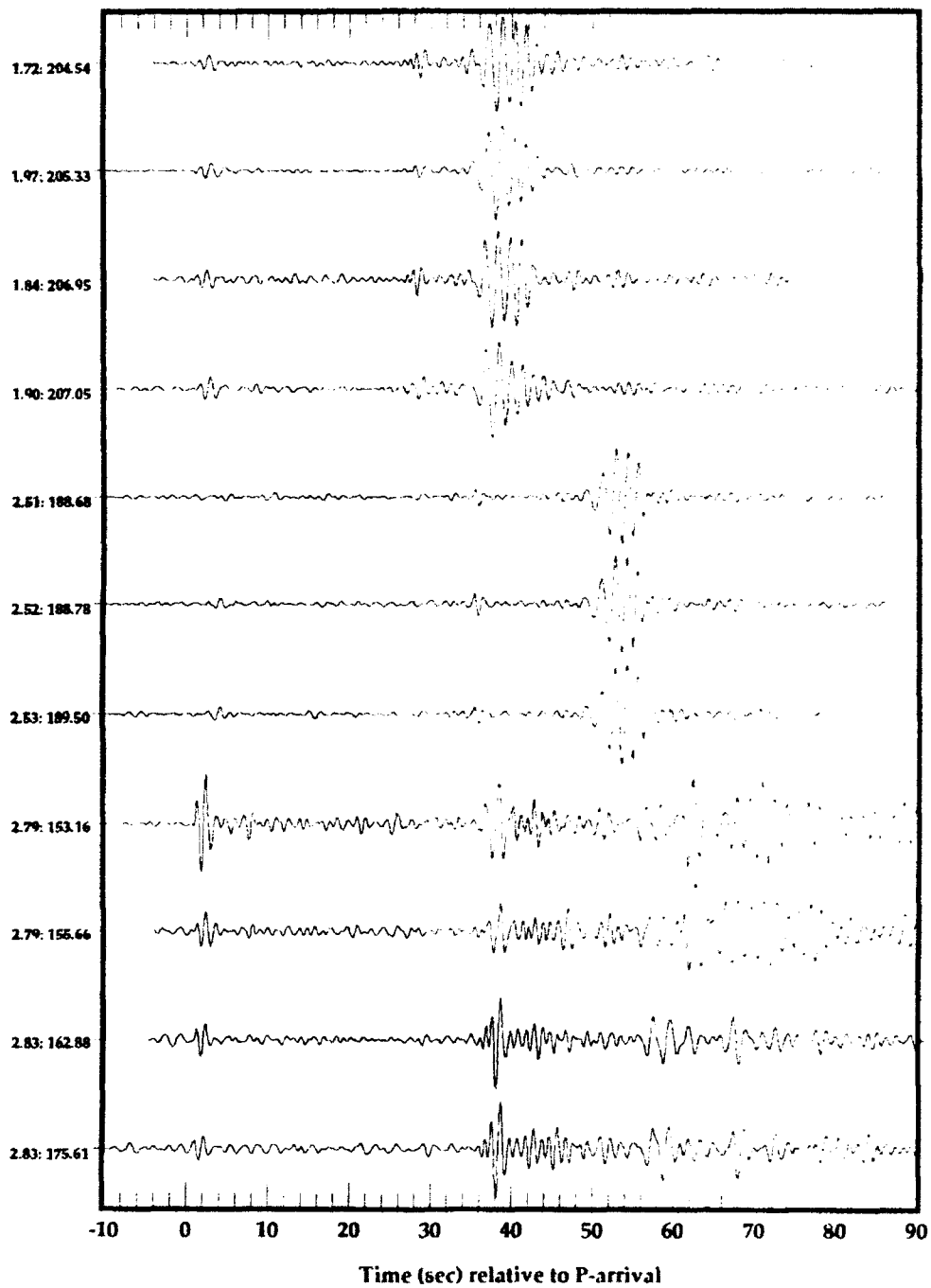


Figure 7b. 0.5 to 1.0 Hz bandpass filtered vertical component seismograms recorded by the borehole instrument at station KKL for events to the south. Distance and back azimuth in degrees are given for each trace.

Figures 7a and 7b show events to the south. These data show an abrupt transition from the southwest quadrant, where strong Rg phases are seen, to the southeast quadrant, which show weak or nonexistent Rg arrivals coupled with an energetic Lg coda. This sudden transition takes place between two events that are at approximately the same distance and are physically close to each other. From Figure 1 we can see that there is the possibility that Lake Balkhash is causing this transition, i.e. all of the events in the southeast quadrant are on the opposite side of the lake as those in the southwest quadrant. We might reasonably expect that Rg would be selectively attenuated across a large lake, however the possibility exists that the southeast events may be small earthquakes at depth and the southwest events may be shallow mining explosions. Another interesting characteristic of this set of events is the remarkable similarity between waveforms that can be seen in the filtered traces. It appears that these 12 events are coming from four different locations.

The data shown here represent a rich source of information that provide us with the means for learning about local and regional wave propagation. In this study we will concentrate on the south event data set for doing the full waveform inversion, although we use all of the non-local data in the quantitative analyses described in the next section.

2.3 Data Analysis

As we have shown, the major difference between the events recorded at KKL is the excitation of Rg and this appears to systematically vary with back azimuth. Synthetic seismograms typically show a strong dependence of Rg amplitude on source depth and this dependence has been proposed as a source depth discriminant. The most serious problem associated with using Rg as a source depth discriminant is that its propagation characteristics are also probably strongly effected by small scale near surface lateral variations in structure. Observations of Rg propagation characteristics for different regions and source-receiver paths will provide important information for

quantifying structural effects and for determining under what circumstances Rg amplitudes and/or dispersion properties can be effective as a source depth discriminant.

Given the potential importance of Rg as a discriminant and its gross behavior as seen in the data, we decided to focus on quantifying Rg propagation characteristics as observed in this data set. We used analysis techniques to determine the Rg dispersion curves as a function of frequency and various Rg amplitude ratios at a fixed frequency.

Figure 8 shows the results of the Rg dispersion curve analysis. These functions were determined from the vertical component seismograms by making time-varying spectral estimation plots, i.e. sonograms, and then measuring the Rg ridge line in cases where it was distinct. Of the 53 non-local events, we were able to see apparent Rg dispersion functions in 32 events. The functions are gray-coded according to the back azimuth and the legend in Figure 8 gives the event back azimuth and distance coordinates. There is a clear and systematic dependence of Rg group velocities on back azimuth with events to the north showing lower group velocities and events to the south showing higher group velocities. Most of the events which failed to show Rg dispersion ridges in the sonograms came from the north. We found a number of events for which the Rg dispersion ridges were fairly clear in the sonograms, yet the Rg phase was difficult to see in either the filtered or unfiltered raw data.

The second analysis technique we used was designed to measure amplitudes of all of the major arrivals, as well as noise, at a fixed frequency. We did this by computing a time-varying envelope function from a Gaussian narrow band filter. The program then picked off the peak amplitudes of the P, S and Rg arrivals along with the peak and mean noise amplitude. An example of the output from this analysis for one of the events to the south is shown in Figure 9. At the top of this figure are the original unfiltered components rotated into radial, transverse and vertical directions. At the bottom is a plot of the three component envelope functions for a frequency of 0.75 Hertz along with the amplitude picks made by the program for P, S and Rg showing

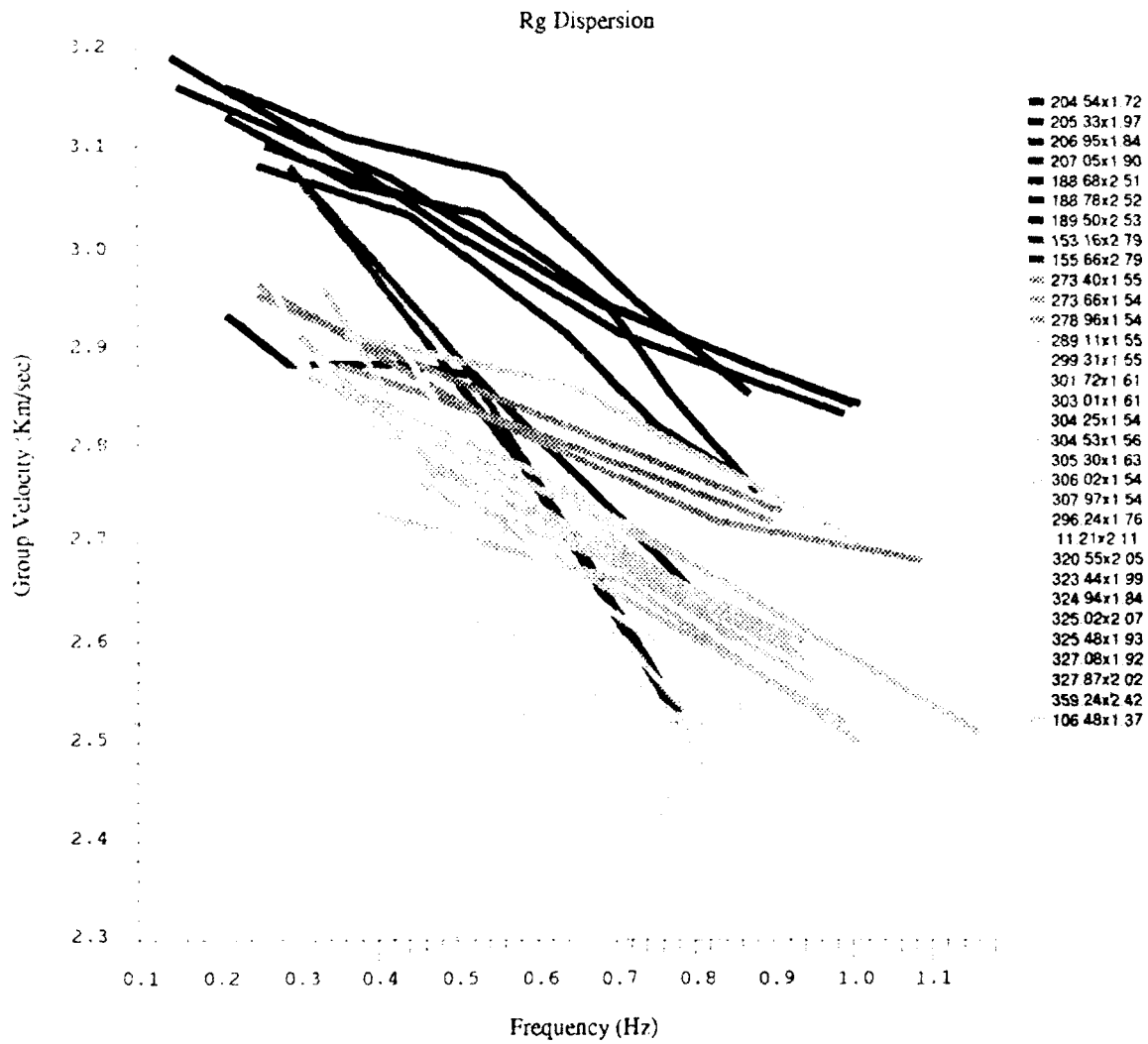


Figure 8. Observed Rg dispersion curves for the non-local events used in this study. The back azimuths and distances in degrees are shown in the legend.

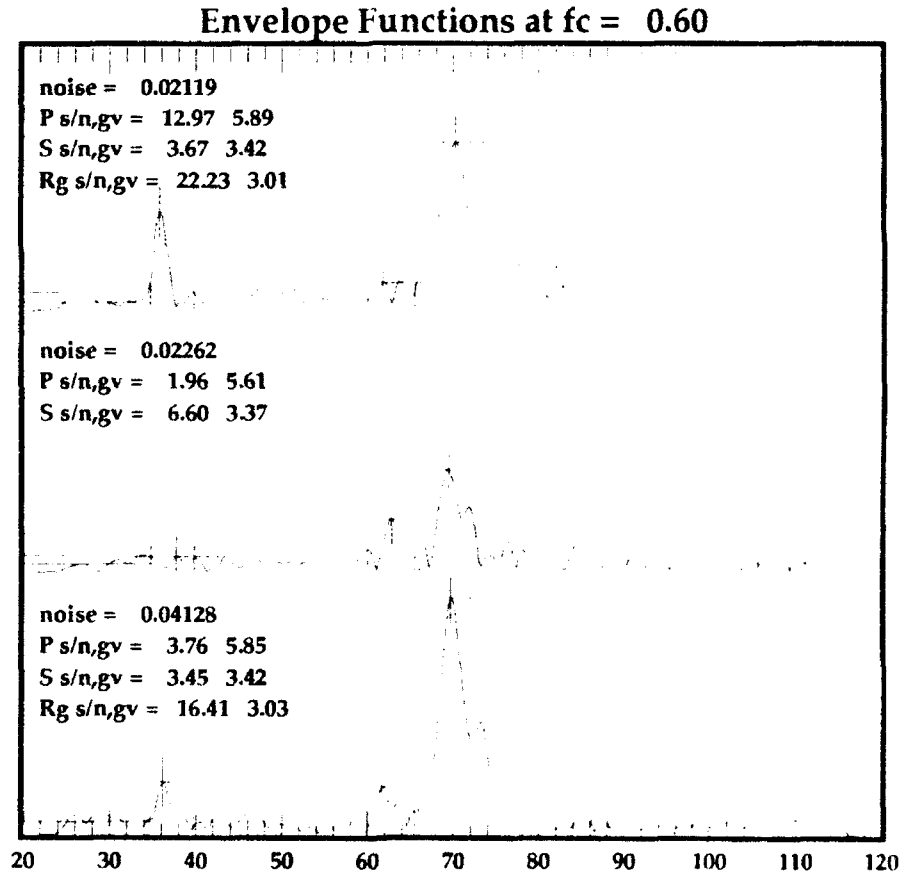
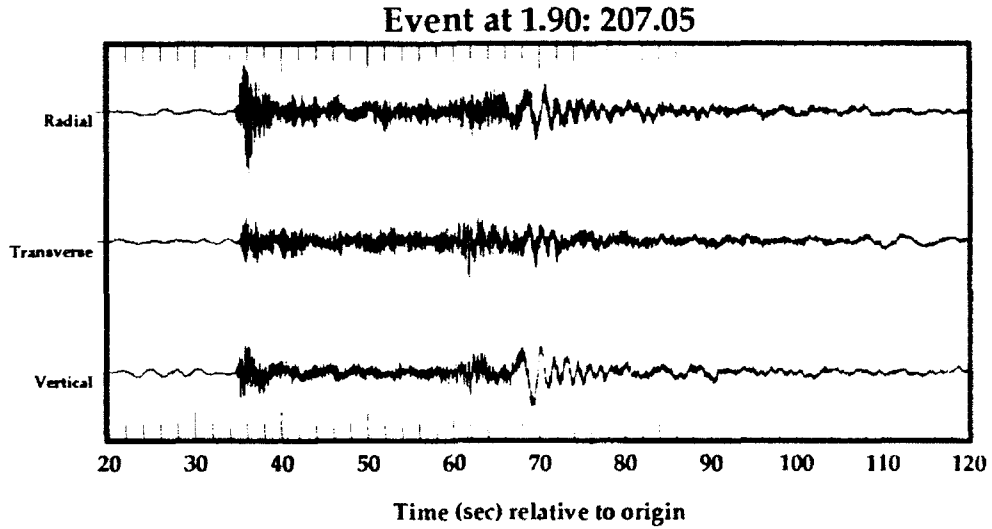


Figure 9. Envelope function processing of an event to the south to determine P, S and Rg group velocities and amplitude levels. These envelope functions were computed at a frequency of 0.6 Hertz.

peak and mean noise levels, and P, S and Rg signal to noise ratios and group velocities. We applied this same analysis to all of the events and generated a table of group velocities and amplitude characteristics for each event.

Figure 10 shows plots of the Rg group velocity at a frequency of 0.75 Hertz as a function of distance and back azimuth for the vertical component. Once again we see a systematic dependence of group velocity on azimuth with the south being fast and the north being slow. There is no apparent relationship between group velocity and distance which precludes the possibility that the azimuth relationship is an aliased form of a distance dependence. Rg signal to noise ratios and Rg signal to P signal ratios are shown in Figure 11 as a function of back azimuth for the vertical component at a frequency of 0.75 Hertz. The Rg amplitude trend with azimuth is approximately the same as the Rg group velocity trend, with high Rg amplitudes to the south and west, corresponding to high Rg group velocities, and low Rg amplitudes to the north and east, corresponding to low Rg group velocities.

The results from these analyses show a wide variability in Rg group velocities and amplitudes. The question that we would like to answer is how much of this variability is due to wave propagation effects and how much is due to source effects, namely source depth. Our knowledge of this region indicates that most, if not all, of these events are shallow mining explosions, although we cannot preclude the possibility that some of these events are small earthquakes. Because we know that there is considerable mining activity to the north of KKL, the low Rg amplitudes of events from this region are most likely due to propagation effects. As we go to the west of north, Rg amplitudes increase until they peak at approximately due west, where we see Rg amplitude ratios of about 100. As we will show in the next sections, these high Rg amplitude ratios indicate a clean and efficient propagation path between source and receiver and they also indicate very shallow source depths. In these situations Rg can be used to clearly discriminate between man-made, shallow sources and natural, deeper

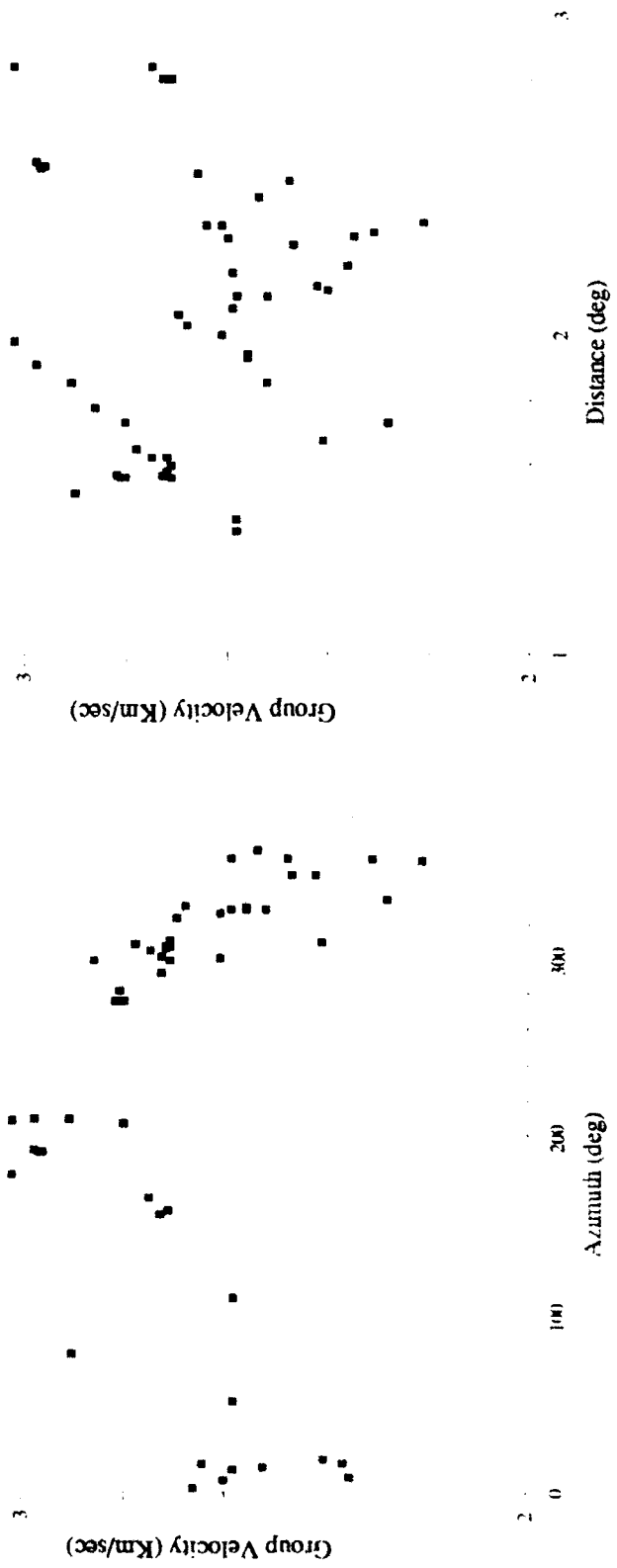


Figure 10. Vertical component Rg group velocities vs. back azimuth and distance at a frequency of 0.6 Hertz.

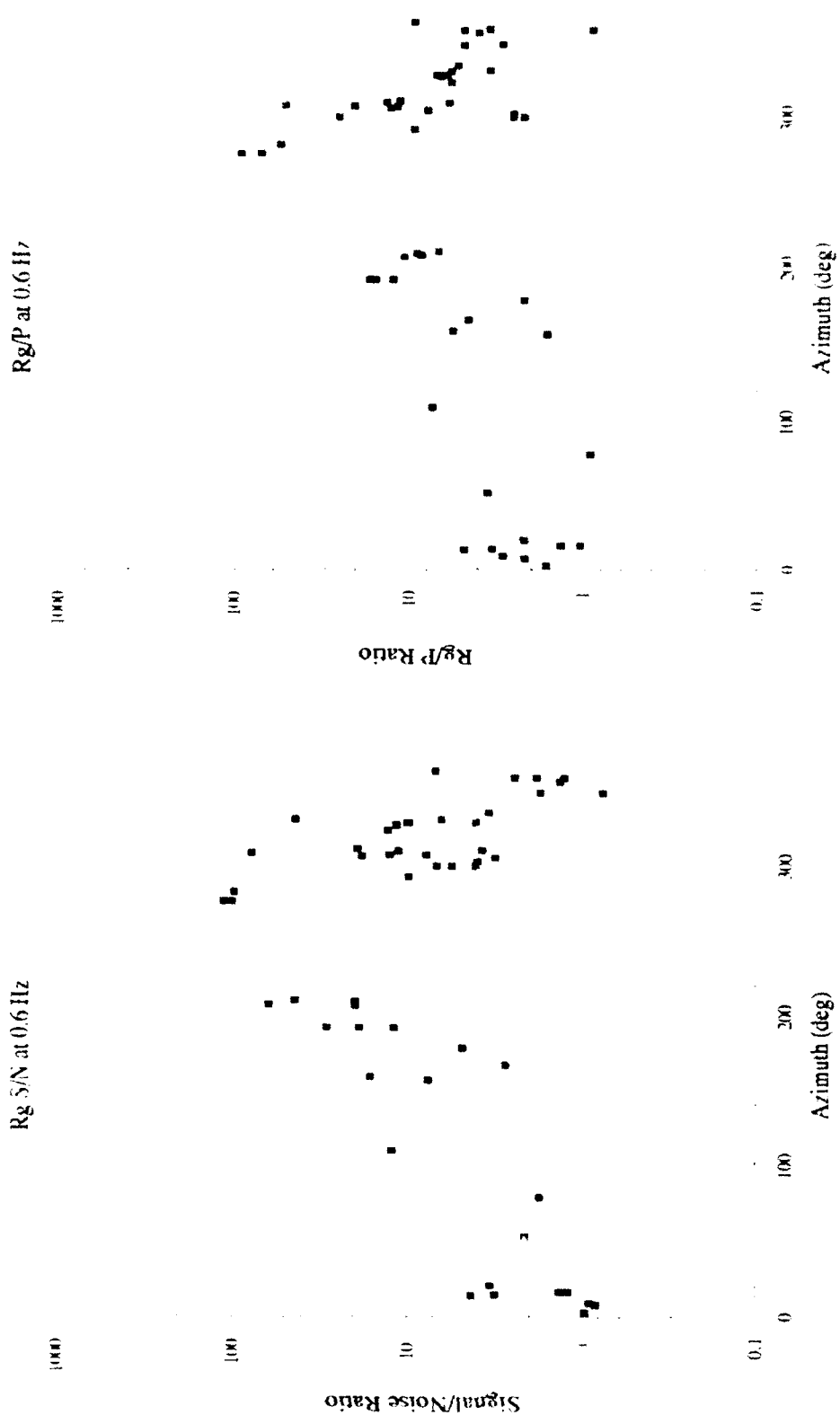


Figure 11. Vertical component Rg signal to peak noise ratio and Rg to P amplitude ratio vs. back azimuth at a frequency of 0.6 Hertz.

sources. The events to the south of KKL show an interesting abrupt transition from strong and fast Rg arrivals in the southwestern quadrant to weaker and slower Rg arrivals in the southeastern quadrant.

3. Inversion Process

We developed both dispersion and full waveform inversion tools for determining earth structure and source parameters. These tools were based upon the cylindrical geometry, laterally homogeneous, elastic wave propagation methods developed by Harvey² that use a normal mode superposition approach for computing synthetic seismograms. Because of concerns that have been raised about the viability of the perturbation approximation used in this method for computing the effect of anelastic attenuation,³ we checked our final solutions with a reflectivity based method that follows the work of Luco, et. al.⁴ We found that the approximations made in the normal mode method had no appreciable effect on the final solutions given in this report.

3.1 Rg Dispersion Inversion

As a first step in determining earth structure we inverted for P and S velocities using the 32 measured Rg dispersion curves shown in Figure 8. We used a locally developed dispersion inversion code that was based upon a simple damped steepest descent path to minimize the comparison variances. The group velocity structure parameter derivatives were computed analytically in the same manner as the computations of the Q derivatives.

² Harvey, D. (1981). Seismogram synthesis using normal mode superposition: the locked mode approximation. *Geophys. J. R. Astr. Soc.* **66**, 37-61.

³ Day, S., McLaughlin, K., Shkoller, B. and Stevens, J., 1989. Potential errors in locked mode synthetics for anelastic earth models, *Geophysical Research Letters*, v. 16, p. 203-206.

⁴ Luco, J. and Apsel, R. (1983). On the Green's functions for a layered half-space: Part I. *Bull. Seismol. Soc. Am.* **73**, 909-929.

We found that it was easy to match the short Rg dispersion curve segments that we measured and that the major problem in the inversion was over-parameterization of the structure. In particular, the inversion tended to trade off P and S velocities to produce unphysical results. Also, we found that only a few layers were necessary to produce good fits between theoretical and observed dispersion curves.

By looking at the depth dependence of the eigenfunctions, we determined an approximately optimal depth sampling that resulted in a geometric distribution of layer thicknesses with depth: 0.5, 1.0, 2.0, 4.0, 8.0 km. Fixing these thicknesses, we allowed the P and S velocities to vary in the inversion. We quickly encountered stability problems with the P and S velocity inversions and we fixed these problems by imposing a constant Poisson ratio constraint on each of the layers. This resulted in a maximum of five free parameters which we found to work very well.

The results of the dispersion curve inversion can be seen in Figure 12. The P velocities of the top four layers are all plotted as a function of event back azimuth. The systematic increase of velocity to the south of the station can be most clearly seen in the second layer from the top with the topmost layer showing relatively large and erratic velocity variations and the deeper layers showing more uniform velocities with smaller variance. We can see from this figure that large changes in Rg dispersion characteristics can result from reasonable velocity variations in the very near surface region (down to 10 km depth).

3.2 Full Waveform Inversion

The full waveform inversion method we developed is similar to the method described in Gombert and Masters⁵ and generally consists of the usual damped

⁵ Gombert, J. and Masters, T., 1988, Waveform modelling using locked-mode synthetic and differential seismograms: application to determination of the structure of Mexico, *Geophys. J. R. Astr. Soc.*, **94**, 193-218.

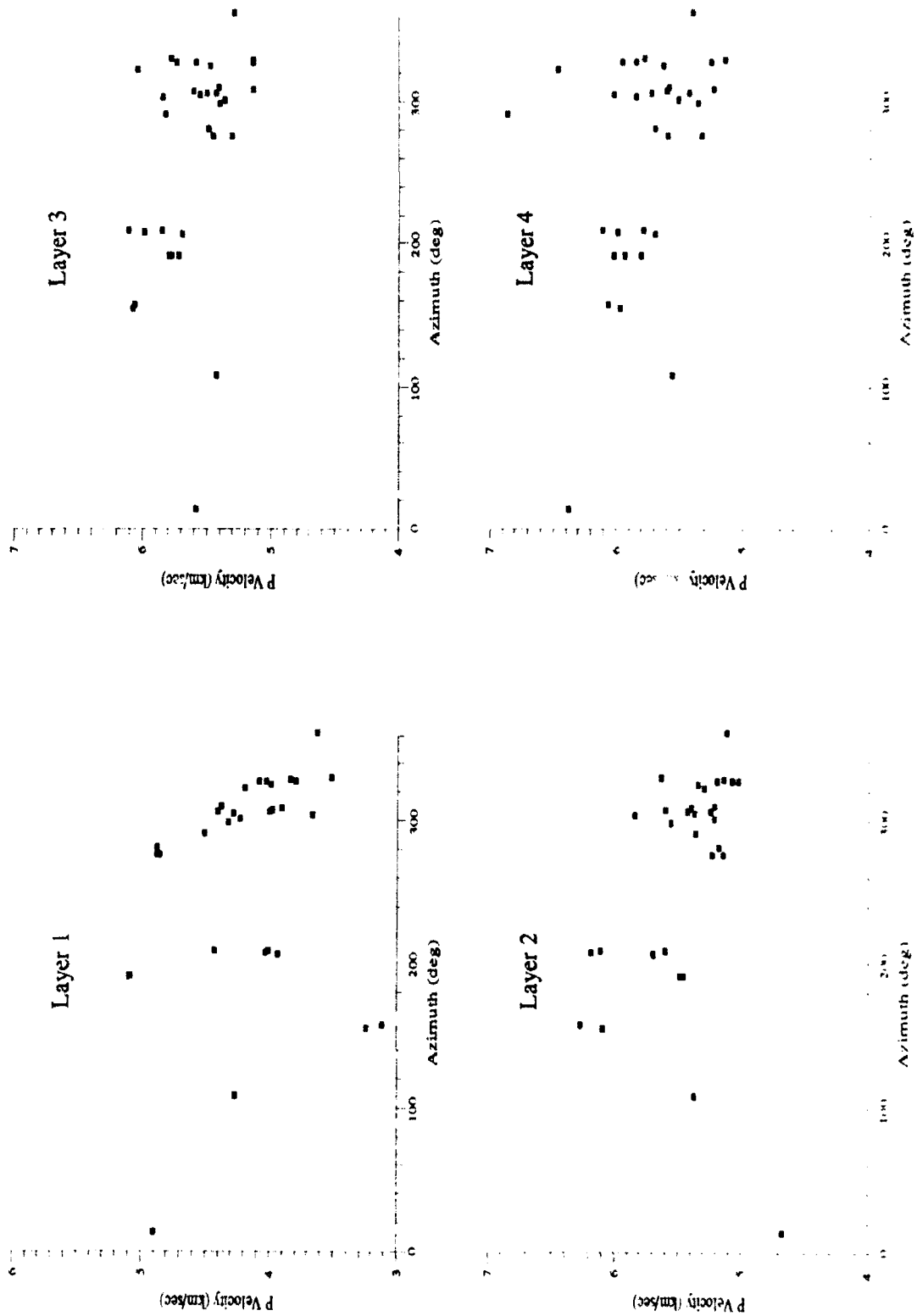


Figure 12. P velocity Rg dispersion inversion results for the top four layers as a function of back azimuth. Layer 1 is the topmost layer of 0.5 km thickness, layer 2 is 1.0 km thickness, layer 3 is 2.0 km thickness and layer 4 is 4.0 km thickness.

steepest descent approach that utilizes differential seismograms⁶ for the determination of local performance function gradients. The inversion parameters consisted of P and S velocities, P and S Q values and source moment tensor. Source depth, source-receiver distance, and layer thicknesses were fixed during the inversion.

We found inverting seismograms in the 0.5 to 1.0 Hertz band to be an extremely non-linear process that required many iterations. As with the dispersion inversion, it was very important for the model to be properly parameterized in order to stabilize the inversion. The waveform inversion code we developed allowed the researcher to specify many different constraints, including P/S velocity ratio constraints and Q_v/Q_p ratio constraints, and to fix or free any of the velocities or Q values for any layer. Other parameters could be specified as well, such as inversion damping parameters. Source moment inversion was done separately and fixed during structure inversion iterations.

Because of the inherent instabilities in the non-linear inversion and the resulting large numbers of iterations that are necessary before convergence, the rapid and accurate calculations of synthetic seismograms along with their derivatives are critical. In the end, we found that 20 to 100 iterations were usually required to find a solution. The inversion code we developed could perform an iteration in about 5 seconds for a single mode, in less than a minute for a dozen modes and in several minutes for a complete locked mode set up to 2 Hertz.

We developed a procedure for performing the inversions which allowed the data to be fit in stages. The first stage involved refining the topmost 10 km of structure by directly fitting Rg waveforms with synthetic results from the fundamental Rayleigh mode. We started with the models determined from the dispersion function inversion

⁶ Harvey, D., 1991, Studies of regional wave propagation using differential seismograms and randomized structural models. Final Report, Report no. PL-TR-91-2126, Phillips Laboratory, Air Force Systems Command, ADA247011.

and matched phases directly between the data and the synthetic waveforms. We then adjusted Q values to obtain good amplitude agreements. As with the dispersion inversion, we found that it was usually necessary to constrain P/S velocity ratios and also Q_α/Q_β ratios. Figure 13 shows a typical fit of observed and synthetic Rg for an event to the south of KKL along with the structure. As we can see from this figure, the fit between the synthetics and data are very good. We had no difficulties in obtaining similar fits for all events in which Rg was clearly visible in the data, however many of the resulting structural models showed unphysical characteristics that we interpreted as being due to poor data constraints on the structural parameters.

In the second stage we used all modes that would be normally trapped by the Moho which resulted in about 12 modes at 1 Hertz and produced both S phases and Rg. In this case we started with the structure obtained from stage 1 along with a starting crustal structure which was the same as the one we used for locating the events. We constrained the upper velocities and all P velocities and Q values and determined the crustal S velocities by fitting the S arrival portion of the seismograms. Fitting of body phases required a two step process which started with a seat-of-the-pants adjustment of velocities to produce an approximate lineup of the data and synthetic arrivals followed by normal inversion iterations to tune the structural model. The main objective of this stage was to obtain good phase agreement of the S arrival between the real and synthetic seismograms.

The crustal P velocities were determined in a similar fashion in the third stage. We put a cap layer at about 150 km depth and included all trapped normal modes. In this stage we constrained all S velocities and inverted for P velocities above the near surface zone.

In the fourth stage we refined amplitudes by allowing the Q values to be unconstrained and in the fifth and final stage we fine-tuned the final results by allowing all parameters to be unconstrained. As a part of the final stage we also determined source

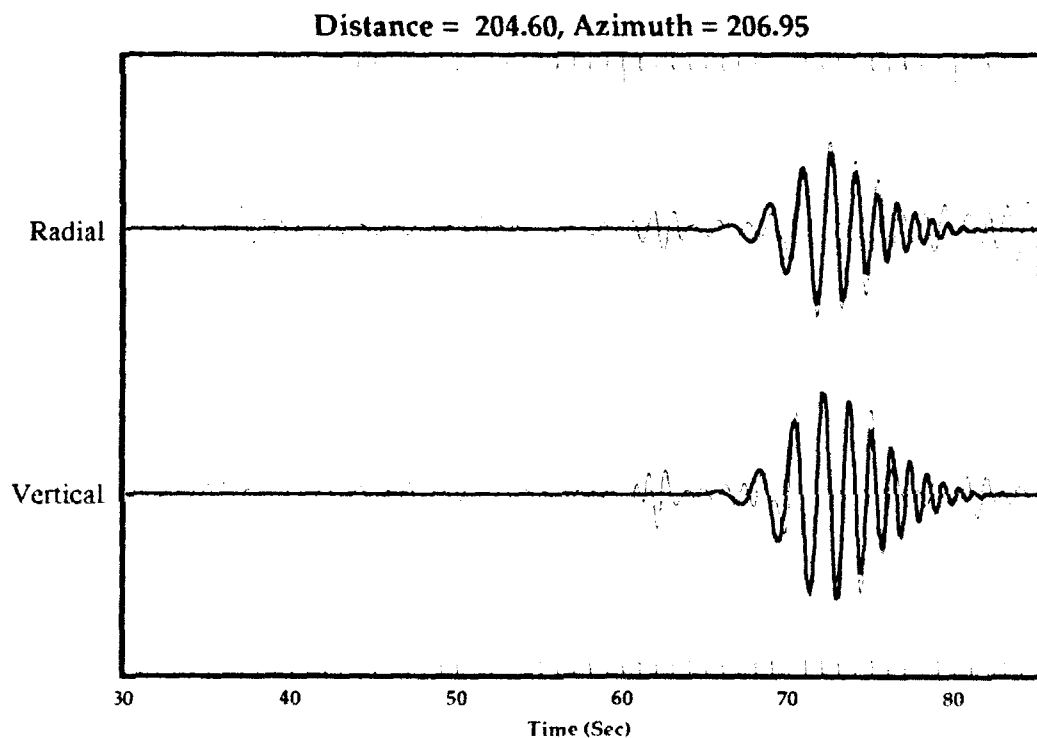
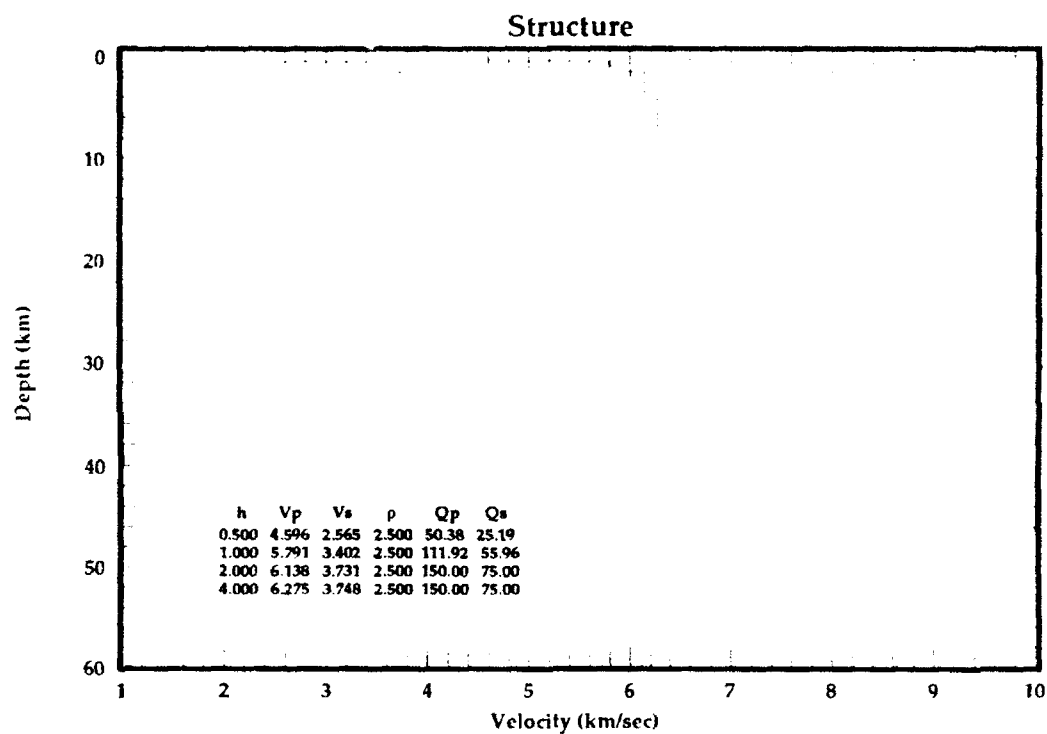


Figure 13. Final results of full waveform inversion using the fundamental mode only and the upper four layers of the structure. The bold traces are the synthetic seismograms and the lighter traces are the real data.

moment parameters.

4. Inversion Results and Application to Other Events

We chose an event to the south of KKL that was one of a cluster of 4 closely spaced events as our first candidate for inversion. This was a typical event in this region with an energetic Rg arrival and clearly identifiable P and S phases. As with all of the results shown in this report, we applied a 0.5 to 1.0 Hertz bandpass filter to the data to reduce the noise below 0.5 Hertz and to low pass filter the data at 1.0 Hertz for comparison with the synthetic seismograms. It was our original hope to start the inversion at a lower frequency band, however the high noise levels below 0.5 Hertz for most events in this data set precluded this possibility.

The first stage inversion results were shown previously in Figure 13. This level of fit between the synthetic and observed Rg phases was typical of the fits for other events. The inversion results obtained by fitting the S phase along with Rg are shown in Figure 14. We see remarkably good agreement between the vertical synthetic and observed waveforms and fairly good agreement on the radial component. The final results using all locked modes with a cap layer at 150 km depth are shown in Figure 15. The Rg fits are unchanged from the previous stages, the S wave fits are, for the most part improved, and the P wave fits are very good.

The results of full waveform inversion for structure and source parameters shown in Figure 15 are remarkable. The overall fit of observed to theoretical waveforms is extremely good, matching both the phase and amplitude characteristics of all of the identifiable arrivals. This fit was obtained with a simple explosion source at a shallow depth (20 m) and the resulting structure is reasonable. Q values are relatively high when compared against those of the Western US, although they are reasonable for shield regions.

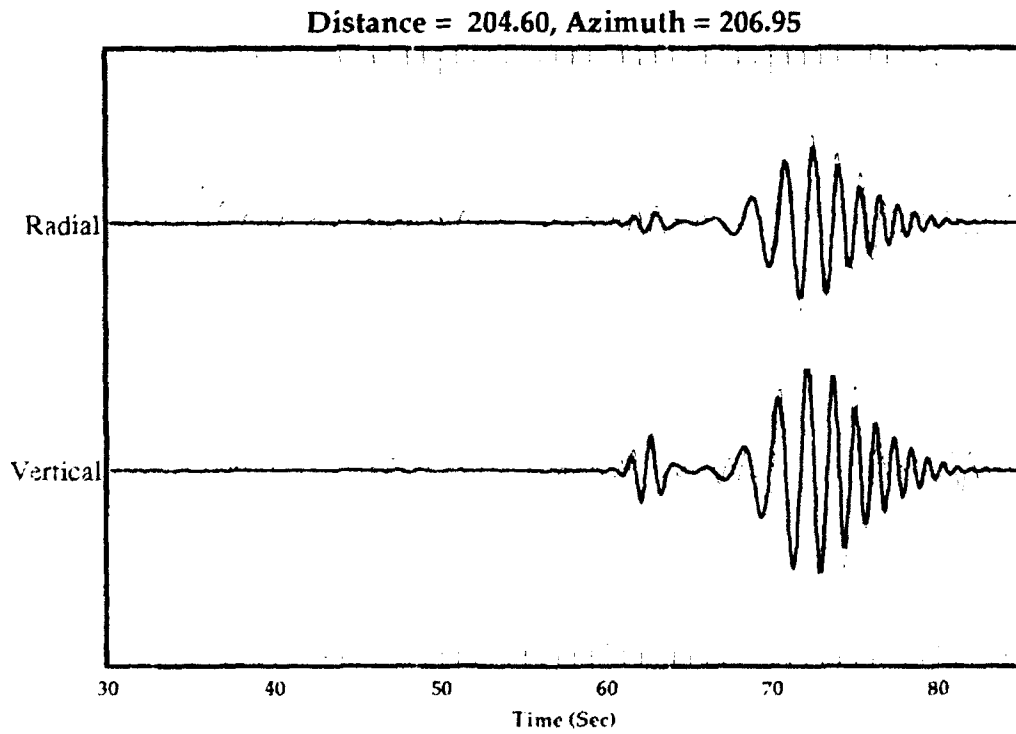
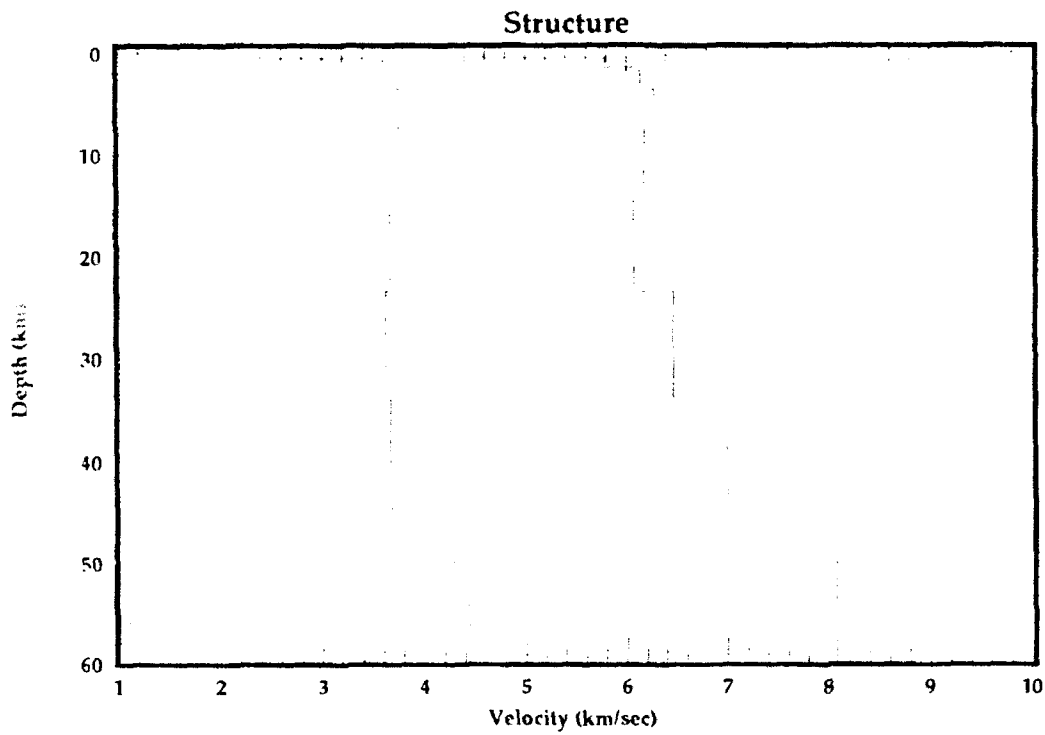


Figure 14. Final results of full waveform inversion using only the modes trapped within the crust. Both Rg and S arrivals are represented in this mode sum. The bold traces are the synthetic seismograms and the lighter traces are the real data.

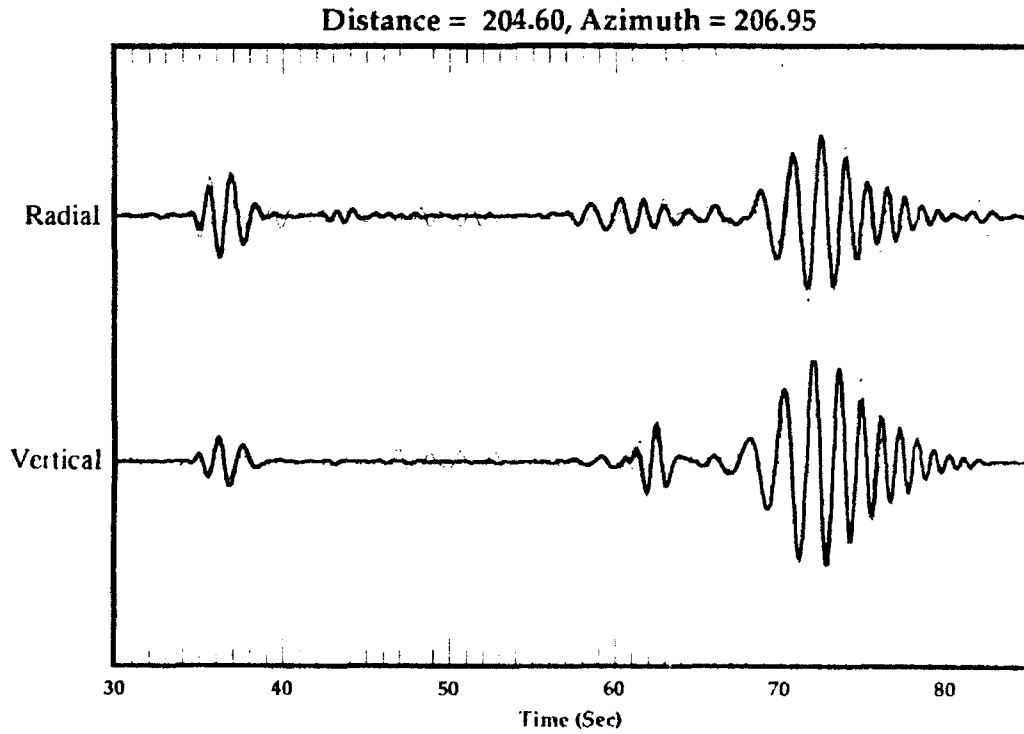
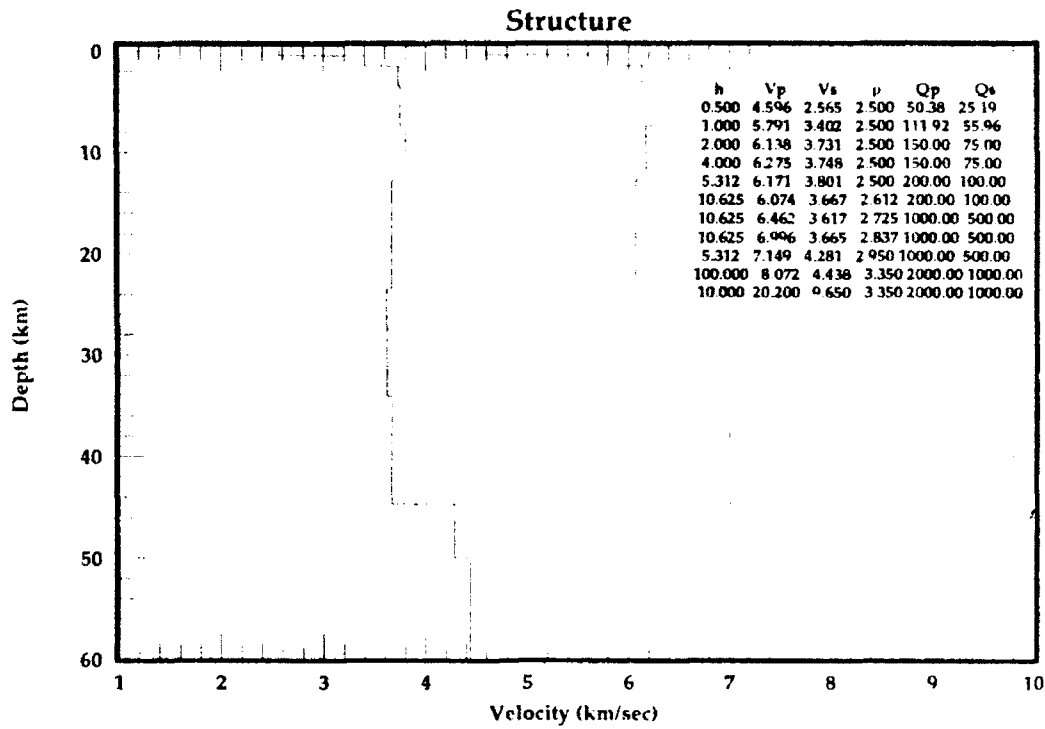


Figure 15. Final results of full waveform inversion using all locked modes trapped by a cap layer at 150 km depth. Complete seismograms are represented in this mode sum including P, S and Rg arrivals. The bold traces are the synthetic seismograms and the lighter traces are the real data.

In order to check the validity of these inversion results, we compared synthetic seismograms with the observations for the other events in the cluster, using the structural parameters obtained from the inversion. In our first attempt at this, we noticed that the overall amplitudes agreed nicely although there were obvious phase errors that appeared to be due to small mis-locations of the events. We adjusted the event locations to produce the best fit between the theoretical and observed seismograms and these results can be seen in Figure 16. These data fits are almost as good as the original inversion event indicating that the inverted structure does a good job in predicting seismic waveforms in the vicinity of the event cluster.

An important and interesting aspect of the results shown in Figure 16 is that waveform inversion can be used to constrain locations in sparse network situations as can be seen in Table 1.

Table 1. Source-receiver distances from travel time and waveform inversion.	
travel time distances	waveform inversion distances
204.6	204.6
191.2	205.5
219.0	205.0
211.3	203.0

The total spread of distances was reduced from 27.8 km to 2.5 km with the latter figure more typical of a mining operation.

Using the same structure we compared theoretical and observed seismograms for three clustered events almost due south of KKL and these comparisons are shown in Figure 17. We did not try to adjust the distances for these events. The P and Rg timing and the Rg dispersion match well between the seismograms, but the synthetic S arrival is late and there is a relatively strong phase on the synthetic radial components that is not seen in the data. The Rg to P amplitude ratio is somewhat larger in the observations than in the synthetics and the Rg to S amplitude ratio is about the same. These events are not in the immediate vicinity of the event that was used to determine the

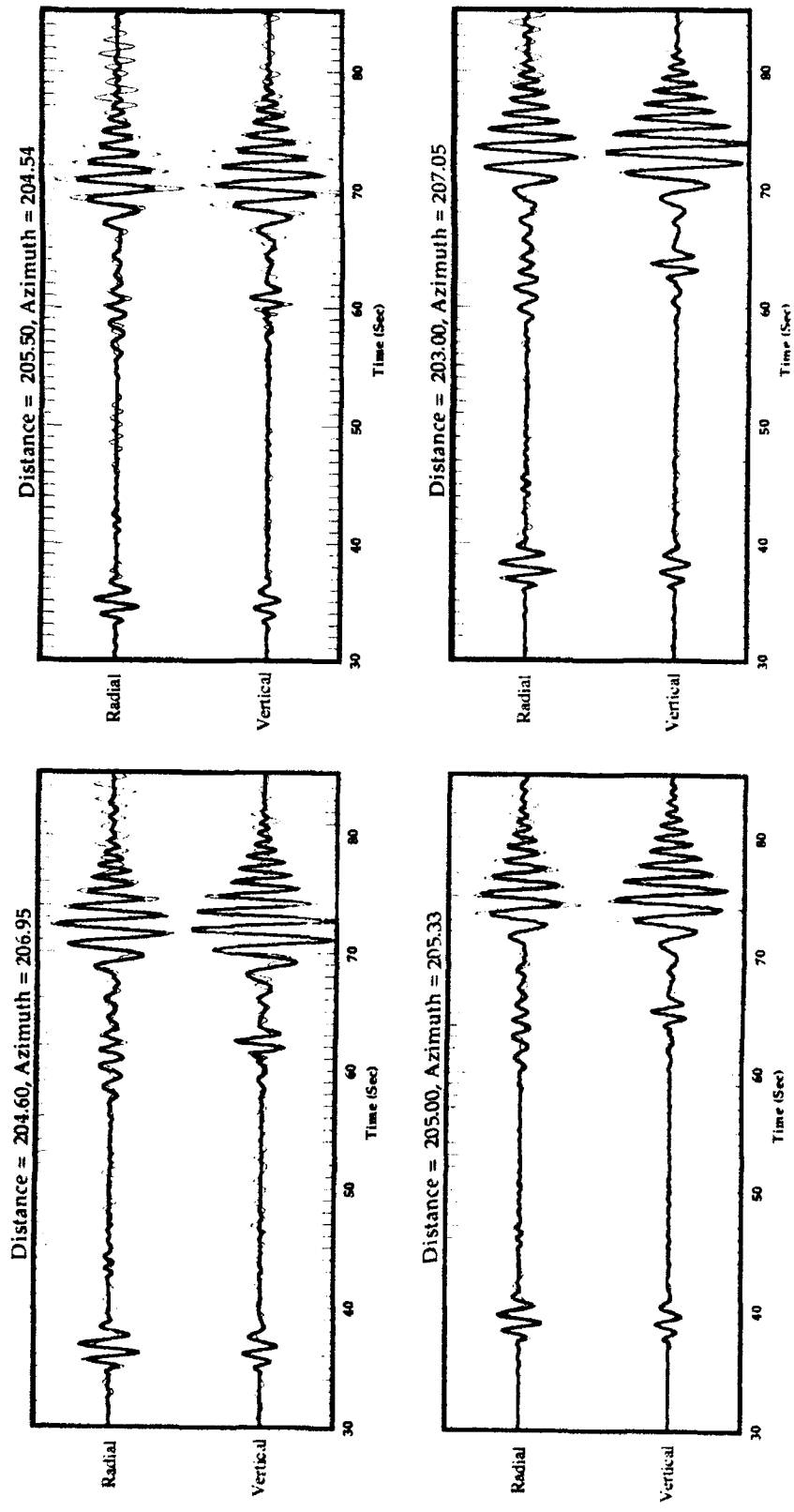


Figure 16. Comparisons of theoretical (heavy lines) and observed (light lines) seismograms for four clustered events southwest of KKL. The structural model given in figure 15 was used for all synthetic seismograms. Source-receiver distances and origin times were adjusted to obtain an optimal fit.

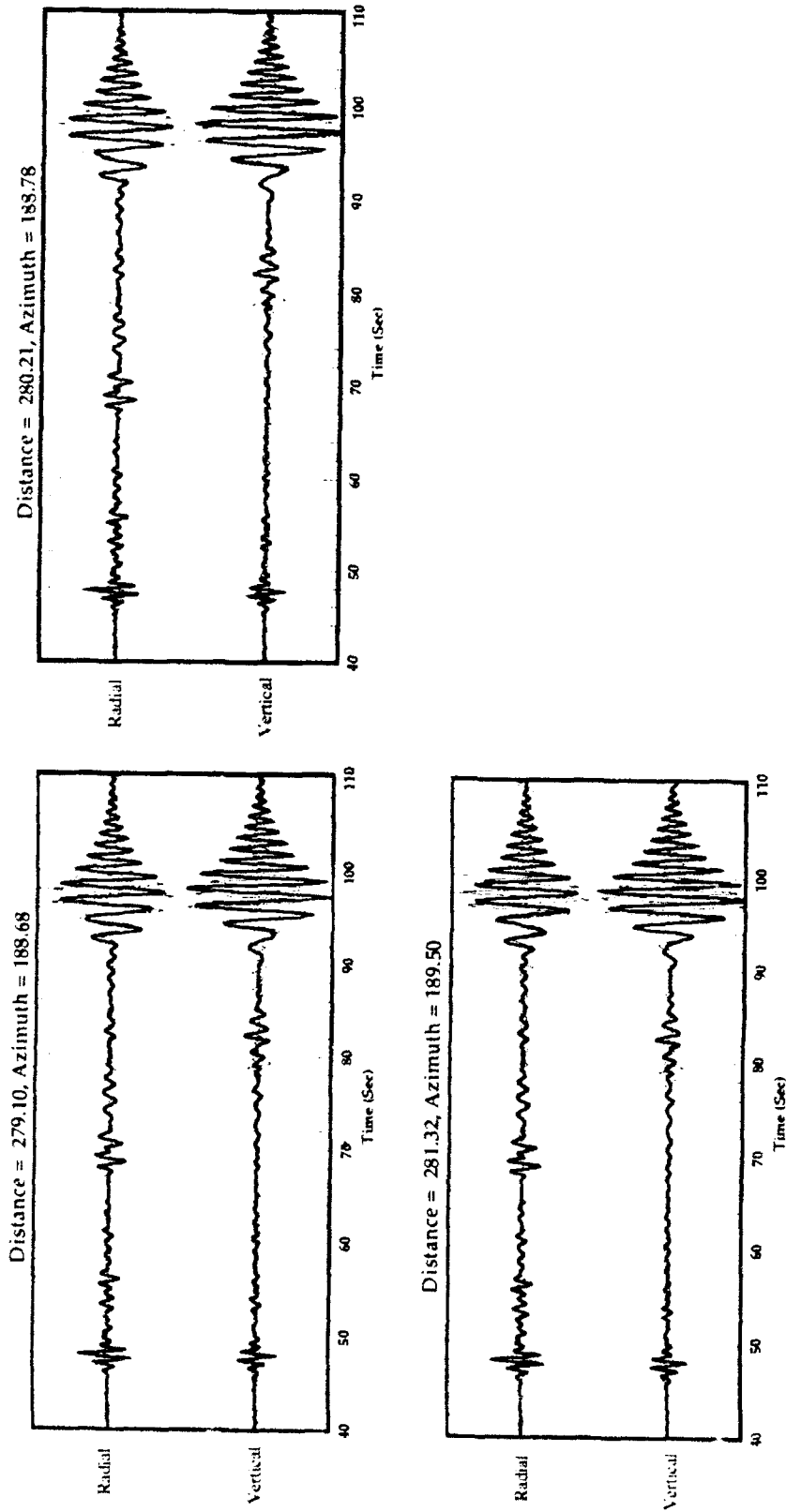


Figure 17. Comparisons of theoretical (heavy lines) and observed (light lines) seismicograms for three clustered events south of KKL. The structural model given in figure 15 was used for all synthetic seismicograms.

structure, however the fits between theoretical and observed traces are quite good. Some minor tuning of the structure parameters would most likely improve the fit significantly.

The four events to the southeast of KKL are shown in Figure 18. When looking at the data, there appears to be an abrupt transition in the waveforms to the southwest of KKL and those to the southeast of KKL. This is reflected in the poor fits of the observed and theoretical waveforms shown in Figure 18. Once again we used the same structure and a shallow explosion source. The major discrepancies between the data and the synthetics are: strong synthetic Rg phases versus weak or non-existent Rg phases in the data, strong S phases in the data versus weak or non-existent S phases in the synthetics, and energetic coda after the S arrival in the data with no apparent coda in the synthetics.

Since Rg is highly dependent on the near surface structure, we attempted to reduce the Rg amplitude by lowering the Q values for the first four layers of the structural model with Q_n going from about 50 to 40 in the first layer, 112 to 50 in the second layer, 150 to 90 in the third layer and 150 to 100 in the fourth layer (Q_4 was lowered in a similar manner). Although this did bring the Rg amplitudes down to be consistent with the observations, this did not solve the problems with the S arrivals. We decided to try comparing synthetic seismograms from an earthquake at a depth of 5 km with the data and the results are shown in Figure 19 for the event at azimuth 155.66 degrees. This figure also shows the original shallow explosion comparison (a) and the shallow explosion comparison with the lowered near surface Q values (b). We performed a moment tensor inversion on the source to come up with an optimal focal orientation to match the three components simultaneously. We also adjusted the source receiver distance to get the correct S-P time on the synthetics. The double couple source comparison used the original inverted structure model with unaltered Q values.

We can see from Figure 19 that the earthquake source at 5 km depth provides a

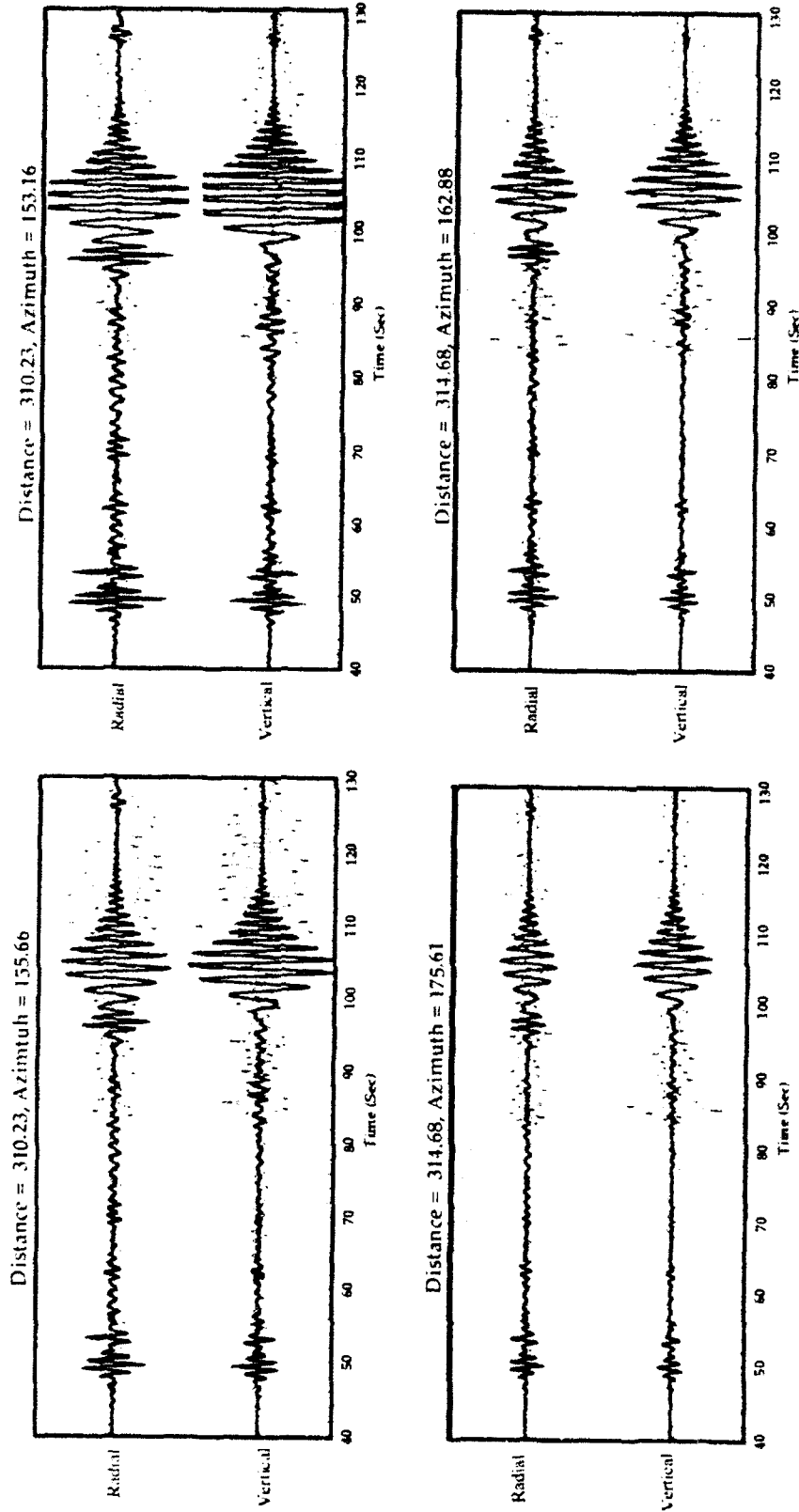


Figure 18. Comparisons of theoretical (heavy lines) and observed (light lines) seismicograms for four events southeast of KKL. The structural model given in figure 15 was used for all synthetic seismicograms.

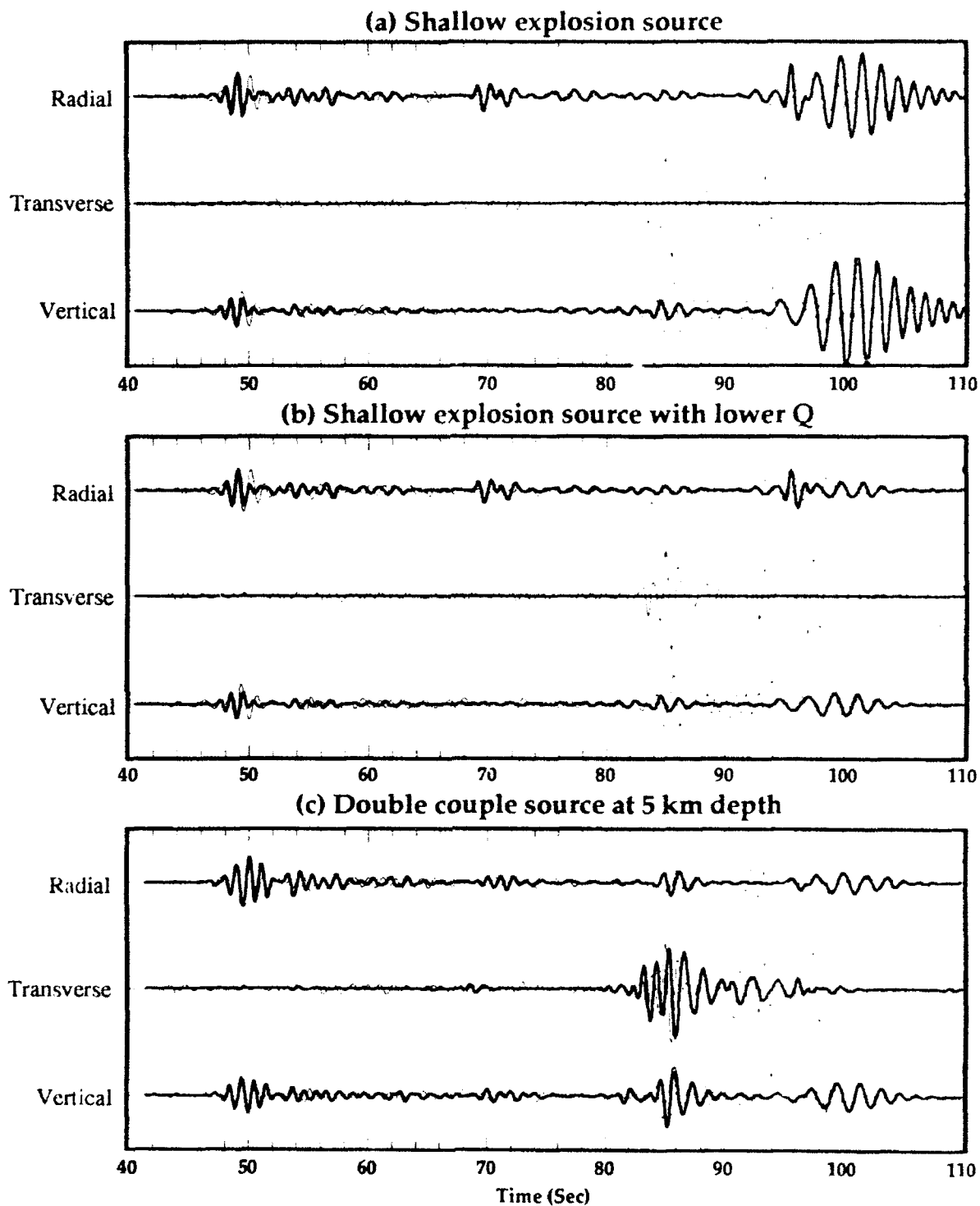


Figure 19. Comparisons of theoretical (heavy lines) and observed (light lines) seismograms for the event southeast of KKL at azimuth 155.66° . The structural model given in figure 15 was used for all synthetic seismograms except for (b) where the near surface Q values were lowered.

very good fit between theoretical and observed waveforms for the P and S arrivals on all three components. In addition, the Rg arrival has been reduced, due to the source depth, without the need for lowering structural Q values. The only portion of the seismogram that we cannot fit well is the trailing coda which could be due to lateral scattering or vertical scattering from fine scale laminations in the crustal structure.⁷ Although we cannot absolutely rule out the possibility that this event is an explosion, we consider the results of this waveform modeling to strongly indicate that this event was a small earthquake.

5. Conclusions

We conducted a two phase study in which we characterized a number of small events in Eastern Kazakhstan in the distance range of 10 to 320 km and we inverted full waveform data for structural and source parameters. We found that there was a strong variability in Rg propagation characteristics as a function of azimuth for the single station we used in this study. We quantified this variability in terms of Rg dispersion function and amplitude characteristics as a function of azimuth. We inverted for near surface structural parameters using observed Rg dispersion and found reasonable azimuthal variations.

We used full waveform inversion to determine structural and source parameters for events to the south of KKL. Although we only performed the structural inversion for one event, we found that the inverted structural model worked well for predicting wave propagation effects for other events in the near vicinity of the event used in the inversion. Waveform inversion was used to refine single station relative locations of presumed mining explosions resulting in a reduction of event clustering from several

⁷ The effects of vertical randomization of the structure on coda are demonstrated in Harvey, D., 1991. Studies of regional wave propagation using differential seismograms and randomized structural models, Final Report, Report no. PL-TR-91-2126, Phillips Laboratory, Air Force Systems Command, ADA247011.

tens of km to several km.

The inverted structural model was used for computing theoretical seismograms for a number of events that were not in the vicinity of the original event cluster used in the inversion. A sudden change in the observed waveforms was successfully modeled by changing the source from a shallow explosion to a 5 km deep double couple. No other changes in the structural parameters were required in order to accomplish this fit.

We have demonstrated the ability to invert full waveform data up to a frequency of 1 Hertz for both structural and source parameters and to produce excellent matches between observed and theoretical seismograms. We have shown that waveform matching can be used to discriminate between small shallow explosions and small relatively shallow earthquakes. Both the Rg and S phases play an important role in this waveform based discrimination. All of these results were obtained using a reasonable and fairly simple structural model with no lateral scattering.

Although we have experienced remarkable success with this particular study, there are many questions that remain unanswered and much more work to be done. We know that lateral scattering will play an important role in certain regions and we suspect that the propagation paths to the north of KKL are strongly influenced by lateral scattering effects. We would like to know more about the mechanisms involved in the scattering. Also this study was conducted using data recorded at a single station and we would like to compare these results with those obtained from other stations. Our suspicion is that Rg strength for shallow sources is a reliable indicator of the presence of weak versus strong lateral scattering in that region. We also suspect that there is a tradeoff between strong Rg and strong S coda (Lg) in the distance ranges used in this study and we theorize that much of Lg coda power is generated by mode conversion of the fundamental Rayleigh mode due to lateral scattering bodies.

The analysis methods documented in this report are well suited for single station data in the frequency range of 0.5 to 1 Hertz which opens up virtually all worldwide

seismic observatories as potential future data sources. We hope to continue this work by looking at data from other regions with different geologic and seismicity settings to further understand and quantify regional wave propagation and to test waveform based methods for discriminating small explosions from earthquakes.

6. Contributing Researchers

No other researchers contributed to the results given in this report.

7. Related Contracts and Publications

No other contracts were used to support the results given in this report.

The following publications were produced in part with support from this contract.

Harvey, D., and Hansen, R., 1991, A Systematic Study of the Effects of Crust and Upper Mantle Structure on Regional Seismograms, Proceedings of the Thirteenth Annual PL/DARPA Seismic Research Symposium, J. Lewkowicz, and J. McPhetres, ed., PL-TR-91-2208, ADA241325

8. References

- Day, S., McLaughlin, K., Shkoller, B. and Stevens, J., 1989, Potential errors in locked mode synthetics for anelastic earth models, *Geophysical Research Letters*, **16**, p. 203-206.
- Gomberg, J. and Masters, T., 1988, Waveform modelling using locked-mode synthetic and differential seismograms: application to determination of the structure of Mexico, *Geophys. J. R. Astr. Soc.*, **94**, 193-218.
- Harvey, D., 1981, Seismogram synthesis using normal mode superposition: the locked mode approximation. *Geophys. J. R. Astr. Soc.*, **66**, 37-61.
- Harvey, D., 1991, Studies of regional wave propagation using differential seismograms and randomized structural models, Final Report, Report no. PL-TR-91-2126,

Phillips Laboratory, Air Force Systems Command, ADA247011.

Luco, J. and Apsel, R., 1983, On the Green's functions for a layered half-space: Part I.

Bull. Seismol. Soc. Am. 73, 909-929.

Thurber, C., Given, H., Berger, J., 1989, Regional seismic event location with a sparse network: application to Eastern Kazakhstan, USSR, *J. Geophys. Res.* 94, 17767-17780.

Prof. Thomas Ahrens
Seismological Lab, 252-21
Division of Geological & Planetary Sciences
California Institute of Technology
Pasadena, CA 91125

Prof. Keiiti Aki
Center for Earth Sciences
University of Southern California
University Park
Los Angeles, CA 90089-0741

Prof. Shelton Alexander
Geosciences Department
403 Deike Building
The Pennsylvania State University
University Park, PA 16802

Dr. Ralph Alewine, III
DARPA/NMRO
3701 North Fairfax Drive
Arlington, VA 22203-1714

Prof. Charles B. Archambeau
CIRES
University of Colorado
Boulder, CO 80309

Dr. Thomas C. Bache, Jr.
Science Applications Int'l Corp.
10260 Campus Point Drive
San Diego, CA 92121 (2 copies)

Prof. Muawia Barazangi
Institute for the Study of the Continent
Cornell University
Ithaca, NY 14853

Dr. Jeff Barker
Department of Geological Sciences
State University of New York
at Binghamton
Vestal, NY 13901

Dr. Douglas R. Baumgardt
ENSCO, Inc
5400 Port Royal Road
Springfield, VA 22151-2388

Dr. Susan Beck
Department of Geosciences
Building #77
University of Arizona
Tucson, AZ 85721

Dr. T.J. Bennett
S-CUBED
A Division of Maxwell Laboratories
11800 Sunrise Valley Drive, Suite 1212
Reston, VA 22091

Dr. Robert Blandford
AFTAC/TT, Center for Seismic Studies
1300 North 17th Street
Suite 1450
Arlington, VA 22209-2308

Dr. Stephen Bratt
Center for Seismic Studies
1300 North 17th Street
Suite 1450
Arlington, VA 22209-2308

Dr. Lawrence Burdick
IGPP, A-025
Scripps Institute of Oceanography
University of California, San Diego
La Jolla, CA 92093

Dr. Robert Burridge
Schlumberger-Doll Research Center
Old Quarry Road
Ridgefield, CT 06877

Dr. Jerry Carter
Center for Seismic Studies
1300 North 17th Street
Suite 1450
Arlington, VA 22209-2308

Dr. Eric Chael
Division 9241
Sandia Laboratory
Albuquerque, NM 87185

Dr. Martin Chapman
Department of Geological Sciences
Virginia Polytechnical Institute
21044 Derring Hall
Blacksburg, VA 24061

Prof. Vernon F. Cormier
Department of Geology & Geophysics
U-45, Room 207
University of Connecticut
Storrs, CT 06268

Prof. Steven Day
Department of Geological Sciences
San Diego State University
San Diego, CA 92182

Marvin Denny
U.S. Department of Energy
Office of Arms Control
Washington, DC 20585

Dr. Zoltan Der
ENSCO, Inc.
5400 Port Royal Road
Springfield, VA 22151-2388

Prof. Adam Dziewonski
Hoffman Laboratory, Harvard University
Dept. of Earth Atmos. & Planetary Sciences
20 Oxford Street
Cambridge, MA 02138

Prof. John Ebel
Department of Geology & Geophysics
Boston College
Chestnut Hill, MA 02167

Eric Fielding
SNEE Hall
INSTOC
Cornell University
Ithaca, NY 14853

Dr. Mark D. Fisk
Mission Research Corporation
735 State Street
P.O. Drawer 719
Santa Barbara, CA 93102

Prof Stanley Flatte
Applied Sciences Building
University of California, Santa Cruz
Santa Cruz, CA 95064

Dr. John Foley
NER-Geo Sciences
1100 Crown Colony Drive
Quincy, MA 02169

Prof. Donald Forsyth
Department of Geological Sciences
Brown University
Providence, RI 02912

Dr. Art Frankel
U.S. Geological Survey
922 National Center
Reston, VA 22092

Dr. Cliff Frolich
Institute of Geophysics
8701 North Mopac
Austin, TX 78759

Dr. Holly Given
IGPP, A-025
Scripps Institute of Oceanography
University of California, San Diego
La Jolla, CA 92093

Dr. Jeffrey W. Given
SAIC
10260 Campus Point Drive
San Diego, CA 92121

Dr. Dale Glover
Defense Intelligence Agency
ATTN: ODT-1B
Washington, DC 20301

Dr. Indra Gupta
Teledyne Geotech
314 Montgomery Street
Alexandria, VA 22314

Dan N. Hagedon
Pacific Northwest Laboratories
Battelle Boulevard
Richland, WA 99352

Dr. James Hannon
Lawrence Livermore National Laboratory
P.O. Box 808
L-205
Livermore, CA 94550

Dr. Roger Hansen
HQ AFTAC/TTR
130 South Highway A1A
Patrick AFB, FL 32925-3002

Prof. David G. Harkrider
Seismological Laboratory
Division of Geological & Planetary Sciences
California Institute of Technology
Pasadena, CA 91125

Prof. Danny Harvey
CIRES
University of Colorado
Boulder, CO 80309

Prof. Donald V. Helmberger
Seismological Laboratory
Division of Geological & Planetary Sciences
California Institute of Technology
Pasadena, CA 91125

Prof. Eugene Herrin
Institute for the Study of Earth and Man
Geophysical Laboratory
Southern Methodist University
Dallas, TX 75275

Prof. Robert B. Herrmann
Department of Earth & Atmospheric Sciences
St. Louis University
St. Louis, MO 63156

Prof. Lane R. Johnson
Seismographic Station
University of California
Berkeley, CA 94720

Prof. Thomas H. Jordan
Department of Earth, Atmospheric &
Planetary Sciences
Massachusetts Institute of Technology
Cambridge, MA 02139

Prof. Alan Kafka
Department of Geology & Geophysics
Boston College
Chestnut Hill, MA 02167

Robert C. Kemerait
ENSCO, Inc.
445 Pineda Court
Melbourne, FL 32940

Dr. Karl Koch
Institute for the Study of Earth and Man
Geophysical Laboratory
Southern Methodist University
Dallas, Tx 75275

Dr. Max Koontz
U.S. Dept. of Energy/DP 5
Forrestal Building
1000 Independence Avenue
Washington, DC 20585

Dr. Richard LaCoss
MIT Lincoln Laboratory, M-200B
P.O. Box 73
Lexington, MA 02173-0073

Dr. Fred K. Lamb
University of Illinois at Urbana-Champaign
Department of Physics
1110 West Green Street
Urbana, IL 61801

Prof. Charles A. Langston
Geosciences Department
403 Deike Building
The Pennsylvania State University
University Park, PA 16802

Jim Lawson, Chief Geophysicist
Oklahoma Geological Survey
Oklahoma Geophysical Observatory
P.O. Box 8
Leonard, OK 74043-0008

Prof. Thorne Lay
Institute of Tectonics
Earth Science Board
University of California, Santa Cruz
Santa Cruz, CA 95064

Dr. William Leith
U.S. Geological Survey
Mail Stop 928
Reston, VA 22092

Mr. James F. Lewkowicz
Phillips Laboratory/GPEH
29 Randolph Road
Hanscom AFB, MA 01731-3010(2 copies)

Mr. Alfred Lieberman
ACDA/VI-OA State Department Building
Room 5726
320-21st Street, NW
Washington, DC 20451

Prof. L. Timothy Long
School of Geophysical Sciences
Georgia Institute of Technology
Atlanta, GA 30332

Dr. Randolph Martin, III
New England Research, Inc.
76 Olcott Drive
White River Junction, VT 05001

Dr. Robert Masse
Denver Federal Building
Box 25046, Mail Stop 967
Denver, CO 80225

Dr. Gary McCartor
Department of Physics
Southern Methodist University
Dallas, TX 75275

Dr. Bao Nguyen
HQ AFTAC/TTR
130 South Highway A1A
Patrick AFB, FL 32925-3002

Prof. Thomas V. McEvelly
Seismographic Station
University of California
Berkeley, CA 94720

Prof. John A. Orcutt
IGPP, A-025
Scripps Institute of Oceanography
University of California, San Diego
La Jolla, CA 92093

Dr. Art McGarr
U.S. Geological Survey
Mail Stop 977
U.S. Geological Survey
Menlo Park, CA 94025

Prof. Jeffrey Park
Kline Geology Laboratory
P.O. Box 6666
New Haven, CT 06511-8130

Dr. Keith L. McLaughlin
S-CUBED
A Division of Maxwell Laboratory
P.O. Box 1620
La Jolla, CA 92038-1620

Dr. Howard Patton
Lawrence Livermore National Laboratory
L-025
P.O. Box 808
Livermore, CA 94550

Stephen Miller & Dr. Alexander Florence
SRI International
333 Ravenswood Avenue
Box AF 116
Menlo Park, CA 94025-3493

Dr. Frank Pilotte
HQ AFTAC/TT
130 South Highway A1A
Patrick AFB, FL 32925-3002

Prof. Bernard Minster
IGPP, A-025
Scripps Institute of Oceanography
University of California, San Diego
La Jolla, CA 92093

Dr. Jay J. Pulli
Radix Systems, Inc.
201 Perry Parkway
Gaithersburg, MD 20877

Prof. Brian J. Mitchell
Department of Earth & Atmospheric Sciences
St. Louis University
St. Louis, MO 63156

Dr. Robert Reinke
ATTN: FCTVTD
Field Command
Defense Nuclear Agency
Kirtland AFB, NM 87115

Mr. Jack Murphy
S-CUBED
A Division of Maxwell Laboratory
11800 Sunrise Valley Drive, Suite 1212
Reston, VA 22091 (2 Copies)

Prof. Paul G. Richards
Lamont-Doherty Geological Observatory
of Columbia University
Palisades, NY 10964

Dr. Keith K. Nakanishi
Lawrence Livermore National Laboratory
L-025
P.O. Box 808
Livermore, CA 94550

Mr. Wilmer Rivers
Teledyne Geotech
314 Montgomery Street
Alexandria, VA 22314

Dr. Carl Newton
Los Alamos National Laboratory
P.O. Box 1663
Mail Stop C335, Group ESS-3
Los Alamos, NM 87545

Dr. George Rothe
HQ AFTAC/TTR
130 South Highway A1A
Patrick AFB, FL 32925-3002

Dr. Alan S. Ryall, Jr.
DARPA/NMRO
3701 North Fairfax Drive
Arlington, VA 22209-1714

Dr. Richard Sailor
TASC, Inc.
55 Walkers Brook Drive
Reading, MA 01867

Prof. Charles G. Sammis
Center for Earth Sciences
University of Southern California
University Park
Los Angeles, CA 90089-0741

Prof. Christopher H. Scholz
Lamont-Doherty Geological Observatory
of Columbia University
Palisades, NY 10964

Dr. Susan Schwartz
Institute of Tectonics
1156 High Street
Santa Cruz, CA 95064

Secretary of the Air Force
(SAFRD)
Washington, DC 20330

Office of the Secretary of Defense
DDR&E
Washington, DC 20330

Thomas J. Sereno, Jr.
Science Application Int'l Corp.
10260 Campus Point Drive
San Diego, CA 92121

Dr. Michael Shore
Defense Nuclear Agency/SPSS
6801 Telegraph Road
Alexandria, VA 22310

Dr. Robert Shumway
University of California Davis
Division of Statistics
Davis, CA 95616

Dr. Matthew Sibol
Virginia Tech
Seismological Observatory
4044 Derring Hall
Blacksburg, VA 24061-0420

Prof. David G. Simpson
IRIS, Inc.
1616 North Fort Myer Drive
Suite 1050
Arlington, VA 22209

Donald L. Springer
Lawrence Livermore National Laboratory
L-025
P.O. Box 808
Livermore, CA 94550

Dr. Jeffrey Stevens
S-CUBED
A Division of Maxwell Laboratory
P.O. Box 1620
La Jolla, CA 92038-1620

Lt. Col. Jim Stobie
ATTN: AFOSR/NL
110 Duncan Avenue
Bolling AFB
Washington, DC 20332-0001

Prof. Brian Stump
Institute for the Study of Earth & Man
Geophysical Laboratory
Southern Methodist University
Dallas, TX 75275

Prof. Jeremiah Sullivan
University of Illinois at Urbana-Champaign
Department of Physics
1110 West Green Street
Urbana, IL 61801

Prof. L. Sykes
Lamont-Doherty Geological Observatory
of Columbia University
Palisades, NY 10964

Dr. David Taylor
ENSCO, Inc.
445 Pineda Court
Melbourne, FL 32940

Dr. Steven R. Taylor
Los Alamos National Laboratory
P.O. Box 1663
Mail Stop C335
Los Alamos, NM 87545

Prof. Clifford Thurber
University of Wisconsin-Madison
Department of Geology & Geophysics
1215 West Dayton Street
Madison, WI 53706

Prof. M. Nafi Toksoz
Earth Resources Lab
Massachusetts Institute of Technology
42 Carleton Street
Cambridge, MA 02142

Dr. Larry Turnbull
CIA-OSWR/NED
Washington, DC 20505

Dr. Gregory van der Vink
IRIS, Inc.
1616 North Fort Myer Drive
Suite 1050
Arlington, VA 22209

Dr. Karl Veith
EG&G
5211 Auth Road
Suite 240
Suitland, MD 20746

Prof. Terry C. Wallace
Department of Geosciences
Building #77
University of Arizona
Tucson, AZ 85721

Dr. Thomas Weaver
Los Alamos National Laboratory
P.O. Box 1663
Mail Stop C335
Los Alamos, NM 87545

Dr. William Wortman
Mission Research Corporation
8560 Cinderbed Road
Suite 700
Newington, VA 22122

Prof. Francis T. Wu
Department of Geological Sciences
State University of New York
at Binghamton
Vestal, NY 13901

AFTAC/CA
(STINFO)
Patrick AFB, FL 32925-6001

DARPA/PM
3701 North Fairfax Drive
Arlington, VA 22203-1714

DARPA/RMO/RETRIEVAL
3701 North Fairfax Drive
Arlington, VA 22203-1714

DARPA/RMO/SECURITY OFFICE
3701 North Fairfax Drive
Arlington, VA 22203-1714

HQ DNA
ATTN: Technical Library
Washington, DC 20305

Defense Intelligence Agency
Directorate for Scientific & Technical Intelligence
ATTN: DTIB
Washington, DC 20340-6158

Defense Technical Information Center
Cameron Station
Alexandria, VA 22314 (2 Copies)

TACTEC
Battelle Memorial Institute
505 King Avenue
Columbus, OH 43201 (Final Report)

Phillips Laboratory
ATTN: XPG
29 Randolph Road
Hanscom AFB, MA 01731-3010

Phillips Laboratory
ATTN: GPE
29 Randolph Road
Hanscom AFB, MA 01731-3010

Phillips Laboratory
ATTN: TSML
5 Wright Street
Hanscom AFB, MA 01731-3004

Phillips Laboratory
ATTN: PL/SUL
3550 Aberdeen Ave SE
Kirtland, NM 87117-5776 (2 copies)

Dr. Svein Mykkeltveit
NTNT/NORSAR
P.O. Box 51
N-2007 Kjeller, NORWAY (3 Copies)

Dr. Michel Bouchon
I.R.I.G.M.-B.P. 68
38402 St. Martin D'Herès
Cedex, FRANCE

Prof. Keith Priestley
University of Cambridge
Bullard Labs, Dept. of Earth Sciences
Madingley Rise, Madingley Road
Cambridge CB3 0EZ, ENGLAND

Dr. Michel Campillo
Observatoire de Grenoble
I.R.I.G.M.-B.P. 53
38041 Grenoble, FRANCE

Dr. Jorg Schlittenhardt
Federal Institute for Geosciences & Nat'l Res.
Postfach 510153
D-3000 Hannover 51, GERMANY

Dr. Kin Yip Chun
Geophysics Division
Physics Department
University of Toronto
Ontario, CANADA

Dr. Johannes Schweitzer
Institute of Geophysics
Ruhr University/Bochum
P.O. Box 1102148
4360 Bochum 1, GERMANY

Prof. Hans-Peter Harjes
Institute for Geophysics
Ruhr University/Bochum
P.O. Box 102148
4630 Bochum 1, GERMANY

Trust & Verify
VERTIC
8 John Adam Street
London WC2N 6EZ, ENGLAND

Prof. Eystein Husebye
NTNF/NORSAR
P.O. Box 51
N-2007 Kjeller, NORWAY

David Jepsen
Acting Head, Nuclear Monitoring Section
Bureau of Mineral Resources
Geology and Geophysics
G.P.O. Box 378, Canberra, AUSTRALIA

Ms. Eva Johannisson
Senior Research Officer
FOA
S-172 90 Sundbyberg, SWEDEN

Dr. Peter Marshall
Procurement Executive
Ministry of Defense
Blacknest, Brimpton
Reading RG7-FRS, UNITED KINGDOM

Dr. Bernard Massinon, Dr. Pierre Mechler
Societe Radiomana
27 rue Claude Bernard
75005 Paris, FRANCE (2 Copies)